UNDERSTANDING THE GLOBAL EFFECT OF SECONDARY ORGANIC AEROSOL ON SIZE DISTRIBUTIONS IN PAST AND PRESENT CLIMATES

by

Stephen Daniel D'Andrea

Submitted in partial fulfilment of the requirements
for the degree of Master of Science

at

Dalhousie University
Halifax, Nova Scotia
November 2013

TABLE OF CONTENTS

LIST OF TABLES

LIST OF FIGURES

ABSTRACT

Recent research has shown that secondary organic aerosols (SOA) are major contributors to ultrafine particle growth to climatically relevant sizes, increasing global cloud condensation nuclei (CCN) concentrations within the continental boundary layer (BL). This thesis contains two separate studies investigating SOA characteristics and the implications of SOA on global climate. The first study investigates two critical, but uncertain, characteristics of SOA: (1) the amount of SOA available to condense and (2) the volatility or condensational behavior of SOA. The second study investigates the effect of biological volatile organic compound (BVOC) emission changes on SOA formation from preindustrial to present day, and the effect on CCN concentrations using BVOC emission estimates over the last millennium.

While many global models contain only biogenic sources of SOA, recent studies have shown that an additional source of SOA around 100 Tg yr^{-1} correlated with anthropogenic carbon monoxide (CO) emissions may be required to match measurements. Many models also treat SOA solely as semivolatile, which leads to condensation of SOA proportional to the aerosol mass distribution; however, recent closure studies with field measurements show nucleation mode growth can be captured only if it is assumed that a significant fraction of SOA condenses proportional to the Fuchs aerosol surface area (i.e. diffusion-limited condensation). This suggests a very low volatility of the condensing vapors. We explore the significance of these findings under present-day conditions using GEOS-Chem-TOMAS global aerosol microphysics model and observations of aerosol size distributions around the globe. The change in the number concentration of particles of size $D_p > 40$ nm (N40) within the BL assuming surface-area condensation compared to mass-distribution net condensation yielded a global increase of 11% but exceeded 100% in biogenically active regions. The percent change in N40 within the BL with the inclusion of the additional 100 Tg(SOA) yr^{-1} compared to the base simulation solely with biogenic SOA emissions (19 Tg yr^{-1}) both using surface area condensation yielded a global increase of 13.7%, but exceeded 50% in regions with large CO emissions.

Emissions of biological volatile organic compounds (BVOC) have changed in the past millennium due to changes in land use, temperature and CO_2 concentrations. A recent model reconstruction of BVOC emissions over the past millennium predicted the changes in the three dominant SOA-producing BVOC classes (isoprene, monoterpenes and sesquiterpenes). These BVOC changes have largely been anthropogenic in nature, and land-use change was shown to have the most dramatic effect by decreasing isoprene emissions. We use these modeled estimates of these three dominant BVOC classes' emissions from the years 1000 to 1990 to test the effect of anthropogenic changes in BVOC emissions on SOA formation and global aerosol size distributions using GEOS-Chem-TOMAS. With anthropogenic emissions held at present day values and BVOC emissions changed from year 1000 to year 1990 values, N80 decreases of >50% in year 2000 relative to year 1000 were predicted in regions with extensive land-use changes since year 1000. This large decrease in N80 could be a largely overlooked and important anthropogenic aerosol effect on regional climates.

LIST OF ABBREVIATIONS AND SYMBOLS USED

BL	continental Boundary Layer
BVOC	Biological Volatile Organic Compounds
C*	average saturation vapor pressure
CCN	Cloud Condensation Nuclei
CDNC	Cloud Droplet Number Concentration
CO	carbon monoxide
CO_2	carbon dioxide
CTM	Chemical Transport Model
D_p	particle diameter
DMPS	Differential Mobility Particle Sizer
GCM	Global Climate Model
GEOS5	the Goddard Earth Observing System model, version 5
GLOMAP	GLObal Model of Aerosol Processes
GRP	Growth Rate Parameterization
H_2O	water
H_2SO_4	sulfuric acid
IPCC	Intergovernmental Panel on Climate Change
LMB	Log-Mean Bias
MEGAN	Model of Emissions of Gases and Aerosols from Nature
MPI-ESM	Max-Planck Institute Earth System Model
N3	number of particles of size $D_p > 3$ nm
N10	number of particles of size $D_p > 10$ nm
N40	number of particles of size $D_p > 40$ nm
N80	number of particles of size $D_p > 80$ nm
N150	number of particles of size $D_p > 150$ nm
NH_3	ammonia
NO_x	nitrogen oxides ($NO + NO_2 = NO_x$)
NO_3	nitrate
O_3	ozone
OA	Organic Aerosol
OH	hydroxyl radical
R^2	correlation coefficient
SMPS	Scanning Mobility Particle Sizer
SO_2	sulfur dioxide
SOA	Secondary Organic Aerosol
TOMAS	TwO Moment Aerosol Sectional microphysics
VOC	Volatile Organic Compounds

ACKNOWLEDGEMENTS

Funding for this research was provided by NSERC through the Network on Climate and Aerosols Network (NETCARE). I would explicitly like to acknowledge all of my co-authors for their assistance and collaboration on these projects. I would also like to acknowledge my committee members.

Firstly, I would like to thank my supervisor, Professor Jeff Pierce, for his continuous guidance and support. Jeff's unrelenting passion and excitement in atmospheric science has made my adventure through science incredibly insightful and knowledgeable. Also, I cannot thank Jeff enough for his endless leadership and kindness outside of the office.

I would also like to thank my office mates both at Dalhousie University and Colorado State University for their support and friendships. The continuous conversations and coffee runs with Jonathan, Chris, Jason, Ryan, and Kim were an endless source of enjoyment and motivation at Dalhousie, and I can't thank Bonne enough at Colorado State University for her insightfulness and awesomeness. I would also like to send thanks to Robin for his support and friendship while both in the office and on the road.

I would like to thank Tanya, Heather-Ann and Jennifer in the Physics and Atmospheric Science Department at Dalhousie for continually supporting me while in Halifax, and I would also like to thank Jamie and Heather in the Atmospheric Science Department at Colorado State University for making my transition to Fort Collins as smooth and enjoyable as possible.

Finally, I would like to send a special heartfelt thank you to my dad and my brothers for their continuous support and encouragement. They have provided me with endless optimism and inspiration to focus and stay on course. This thesis is dedicated to the memory of my late mother and the unconditional love and support she provided.

CHAPTER 1 INTRODUCTION

1.1 Motivation

One of the most important issues currently impacting humans is global climate change. However, there are many uncertainties in quantifying global climate change. One of the most uncertain factors according to the Intergovernmental Panel on Climate Change (IPCC) Fourth Assessment Report is the effect of anthropogenic aerosols on the radiative forcing on the Earth's climate (IPCC, 2007). Aerosols are liquid or solid particles suspended in the air and range in size from a few nanometers (10^{-9} m) in diameter to several micrometers, μm (10^{-6} m).

Anthropogenic aerosols affect Earth's climate both directly and indirectly. Aerosols directly affect Earth's climate by scattering and absorbing solar and terrestrial radiation and indirectly affect Earth's climate by altering cloud properties. The quantification of the change in radiative forcing due to the direct effect is dependent on aerosol mass and particle number concentrations and particle size (or alternative particle mass and size). However, the number and size of aerosol are both highly variable in space and time. Therefore, spatially and temporally resolved information on the atmospheric burden and radiative properties of aerosols is needed to estimate the changes in the radiative budget due to this direct effect.

The indirect effects of aerosols on climate are due to changes in cloud properties by altering the cloud droplet number concentration (CDNC) within clouds. Cloud droplets are not known to form directly from homogeneous nucleation of water vapor in the atmosphere, but rather are formed on seed aerosol particles. These particles are known as cloud condensation nuclei (CCN). If the liquid water mass in a cloud remains constant, an increase in CCN, and ultimately CDNC, would cause an increase in the reflectivity (albedo) of the cloud due to the increase in total liquid water surface area. Increasing total liquid water surface area in clouds causes more incoming solar radiation to be reflected back to space and will cool the climate (Twomey, 1974, 1977, 1991; Albrecht, 1989). This is known as the cloud albedo effect or the first indirect effect. The estimated uncertainty in the cloud albedo effect spans -0.3 to -1.8 Wm^{-2} (Forster et al.,

2007) and was the most uncertain changes in radiative forcing according to the IPCC Fourth Assessment Report (IPCC, 2007). Increasing CDNC in clouds would have another indirect effect on cloud properties. If the CDNC increases and the total liquid water mass remains constant, then the diameter of the cloud droplets would decrease (Albrecht, 1989). This decrease in diameter inhibits the cloud's ability to precipitate, and increases the lifetime of the cloud itself (which, of course, would alter its liquid water content). This is known as the second indirect effect, or the cloud lifetime effect. Therefore, due to the direct and indirect effects of aerosols, changes in radiative forcing and aerosol-climate impacts are highly dependent on particle size distributions and the number concentration of CCN.

Particle size distributions however, evolve in the atmosphere as a direct result of microphysical processes such as nucleation, condensation, coagulation, primary emissions and deposition. Thus estimating the climatic effects of aerosols due to the evolving particle size distributions and CCN number concentrations involves an understanding of the microphysical processes involved.

1.2 Aerosol microphysical processes

Nucleation and primary emission are the source of particle number to the atmosphere. Nucleation involves gas-to-particle conversion, or creation of molecular clusters from gas-phase constituents. Freshly nucleated particles are formed at sizes of ~1 nm and can occur through binary nucleation of sulfuric acid (H_2SO_4) and water vapor (Kulmala et al., 1998) or through ternary nucleation of H_2SO_4, water vapor and ammonia (NH_3) (Korhonen et al., 1999). However, freshly nucleated stable clusters with diameters ~1nm are generally smaller than primary emitted particles (Kulmala et al., 2000, 2004; Mäkelä et al.,1997.; Vehkamaki et al., 2004), making them susceptible to coagulation (the process by which aerosol particles collide and coalesce) with pre-existing particles. Therefore, for freshly nucleated particles to grow to CCN sizes, they must grow through condensation while avoiding coagulational scavenging. The lifetime of atmospheric aerosols and their impact on climate depends on this competition between the condensational growth and the coagulational scavenging of aerosols. Coagulational

scavenging can be a major sink of nanoparticles in the atmosphere and can have a large impact on aerosol size distributions by shifting the distribution towards larger sizes and decreasing total number. Therefore it is crucial to correctly predict the balance between condensational growth and coagulational scavenging to accurately represent aerosol size distributions.

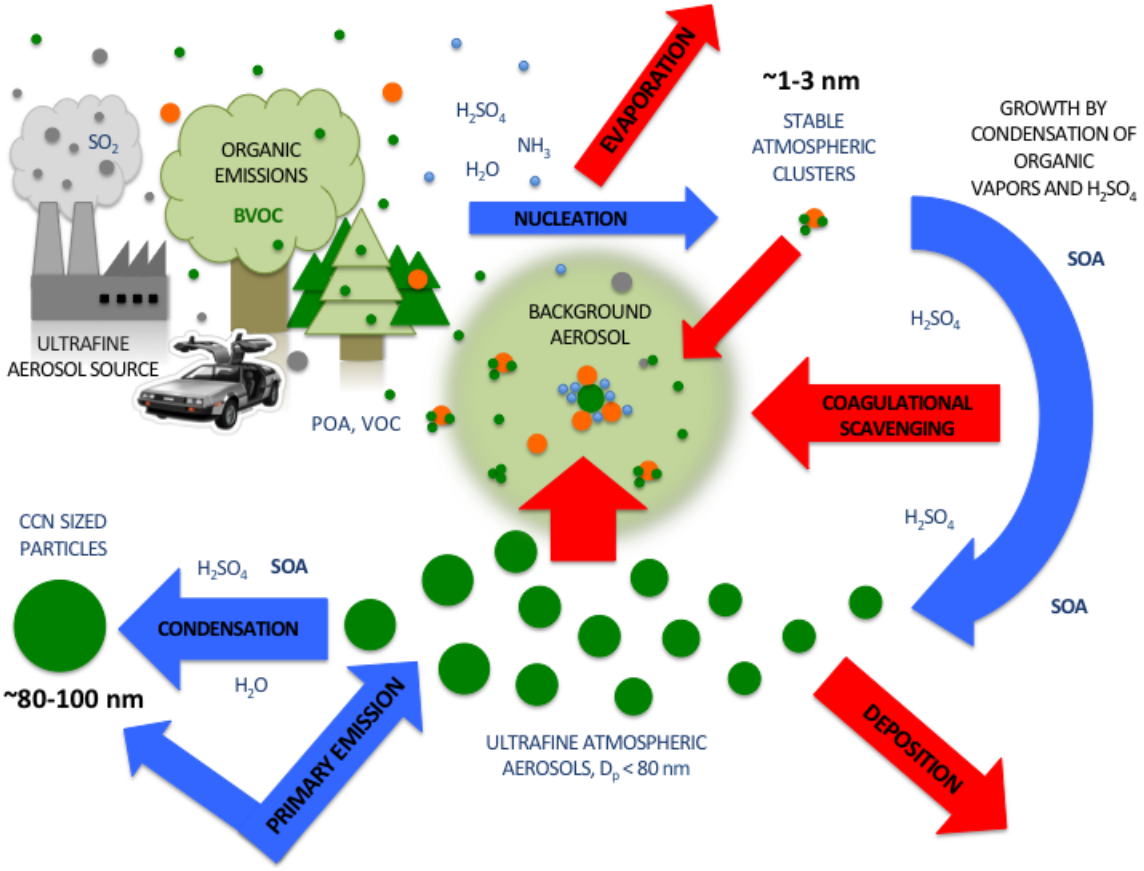

Figure 1.1 Microphysical processes from new particle formation to CCN sized particles.

Figure 1.1 shows the major microphysical processes involved in the evolution of particle size distributions from new particle formation to CCN sized particles. Emissions of ultrafine particles from industrial and biogenic sources are a major source of particles of various sizes, mass and number to the background aerosol in the atmosphere. Nucleation of vapors such as H_2SO_4, NH_3, amines, low-volatility organics and H_2O can create stable clusters with diameters of approximately 1-3 nm. Once stable clusters are

formed through nucleation, condensation of vapors (such as H_2SO_4 and secondary organic aerosol (SOA)) can grow the clusters to larger sizes. These particles can continue to grow via condensation to CCN sized particles with diameters of roughly 50-100 nm. However, the probability of these particles reaching CCN sizes is limited by deposition (wet and dry), evaporation, and coagulational scavenging with the background aerosol. These microphysical processes however, occur over all sized particles, highlighting the importance of understanding these processes and how they affect the growth of freshly nucleated particles to CCN sizes.

Current research indicates that there are multiple factors crucial to understanding the condensational growth of particles in the atmosphere. H_2SO_4 is a well-known contributor to particle growth and is formed in the atmosphere by oxidation of sulfur dioxide (SO_2) (Sipilä et al., 2010). However, recent research indicates that in addition to H_2SO_4, organic vapors significantly impact the condensational growth of particles as well (Riipinen et al., 2011). It has been observed that 20-90% of the total submicron aerosol mass in the atmosphere is comprised of organic aerosol (OA) (Jimenez et al., 2009). A significant contribution to organic aerosol mass burden, ranging from approximately two-thirds of OA mass in rural urban areas to greater than 90% of OA mass in remote areas, are secondary organic aerosols (SOA) (Zhang et al., 2007). Therefore, the condensation of SOA is crucial to growth of particles to CCN sizes. The formation of SOA will be described in the following section.

1.3 Secondary Organic Aerosol

1.3.1 Secondary Organic Aerosol formation

Secondary organic aerosols (SOA) are formed via multistep oxidation of biological volatile organic compounds (BVOCs) emitted from vegetation such as monoterpenes ($C_{10}H_{16}$), isoprene (C_5H_8) and sesquiterpenes ($C_{15}H_{24}$). This oxidation of BVOCs produces lower volatility products and allows partitioning of organic molecules to the particle phase. The formation of SOA results in a major source of condensable material

for particle growth. This is shown schematically in Figure 1.2. Emissions of BVOCs oxidize via the hydroxyl radical (OH), ozone (O_3) and nitrate (NO_3) to form organic precursor gases. These organic precursors can undergo gas-to-particle conversion to create SOA. Growth of aerosols from condensation of SOA to CCN sizes leads to activation of the CCN to form cloud droplets, thus impacting climate through direct and indirect aerosol effects.

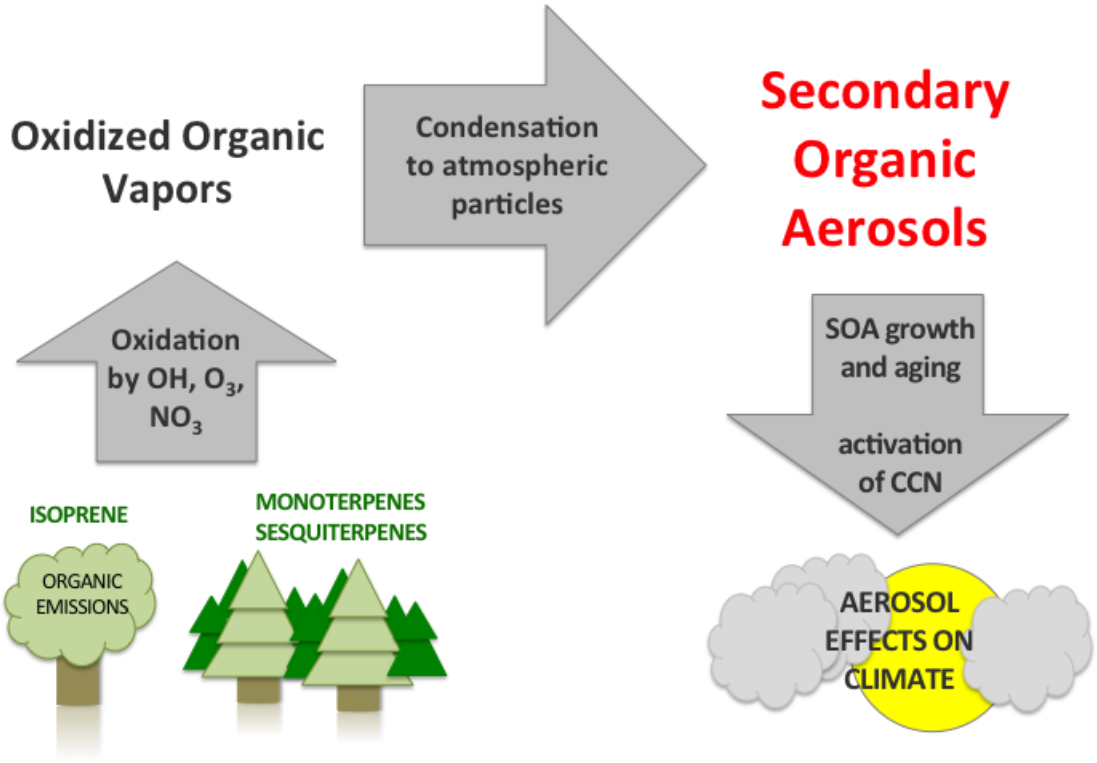

Figure 1.2 Schematic of secondary organic aerosol formation in the atmosphere and the effect on climate.

1.3.2 Modeling of Secondary Organic Aerosol

Global climate models (GCMs) are the primary tool for predicting future climate change, and many modern GCMs include online aerosol microphysics simulations with aerosol-cloud interactions. However, their predictions are highly dependent upon correctly

simulating aerosol size and number. Many aerosol processes in global aerosol models are uncertain and are imperfectly represented in these simulations (Lee et al., 2013). Early modeling studies of SOA have notoriously underpredicted observed SOA concentrations (deGouw et al., 2005; Heald et al., 2005; Volkamer et al., 2006). However, recent studies involving measured OA concentrations, physical properties and chemical properties have begun to close the gap between predicted and measured SOA concentrations (e.g. Spracklen et al., 2011b). In order to understand the climatic effects of SOA, the manner at which SOA affects aerosol size distributions and the microphysical implications must be understood.

This thesis contains two separate studies investigating SOA characteristics and the implications of SOA on global climate. The first study investigates two critical, but uncertain, characteristics of SOA: (1) the amount of SOA available to condense and (2) the volatility or condensational behavior of SOA. The effect of these two characteristics on CCN concentrations is investigated and compared to global boundary layer (BL) observations to validate the accuracy of the SOA assumptions. The second study investigates the effect of BVOC emission changes on SOA formation from preindustrial to present day, and the effect on CCN concentrations using BVOC emission estimates over the last millennium. These BVOC changes are largely anthropogenically driven by land-use changes and CO_2 and temperature increases. This thesis addresses both of these SOA studies by utilizing a global chemical transport model with online aerosol microphysics to represent the evolution of aerosol size distributions.

CHAPTER 2 UNDERSTANDING GLOBAL SECONDARY ORGANIC AEROSOL AMOUNT AND SIZE-RESOLVED CONDENSATIONAL BEHAVIOR *

* D'Andrea, S. D., Häkkinen, S. A. K., Westervelt, D. M., Kuang, C., Levin, E. J. T.,Kanawade, V. P., Leaitch, W. R., Spracklen, D. V., Riipinen, I., and Pierce, J. R.: Understanding and constraining global secondary organic aerosol amount and size-resolved condensational behavior, Atmos. Chem. Phys., 13, 11519-11534, doi:10.5194/acp-13-11519-2013, 2013.

2.1 Introduction

Atmospheric aerosols affect both health and climate. These health and climate effects depend directly on aerosol size and composition. Atmospheric aerosols can influence the climate by scattering incoming solar radiation (Rosenfeld et al., 2008; Clement et al., 2009) as well as acting as nuclei for cloud droplets (Charlson et al., 1992). The influence of aerosols on clouds is driven by the number concentration of cloud condensation nuclei (CCN) (particles on which cloud droplets form generally having dry diameters larger than 30 nm to 100 nm), which is highly dependent on the aerosol size distribution (Dusek et al., 2006; McFiggans et al., 2006; Petters and Kriedenweis, 2007; Pierce and Adams, 2007). Aerosol nucleation, the formation of ~1 nm diameter particles from the clustering of vapors, is likely the dominant source of aerosol number to the atmosphere (Kulmala et al., 2004). However, these particles must grow to CCN sizes, primarily through condensation, in order to affect climate (Pierce and Adams, 2007; Vehkamäki and Riipinen, 2012). Whether or not these particles survive to CCN sizes depends on the competition between condensational growth and coagulational scavenging with the pre-existing aerosol (Kerminen and Kulmala, 2002; Pierce and Adams, 2007; Kuang et al., 2009; Westervelt et al., 2013). Thus, faster particle growth rates allow more particles to survive to CCN sizes.

The condensation of sulfuric acid to freshly nucleated particles is known to be a contributor to the growth of these particles (Sipilä et al., 2010). In recent studies by Riipinen et al. (2011), measured growth rates of ultrafine (diameters smaller than 100 nm) particles in forested regions were much higher than maximum growth rates from sulfuric acid alone. They found through a combination of measurements and modeling that the condensation of low-volatility secondary organic aerosols (SOA) can account for this additional growth. Measurements of the submicron particle composition throughout the continental boundary layer show 20 – 90% of the aerosol is organic, and much of this organic aerosol is SOA (Jimenez et al., 2009). Thus we expect that SOA may be a significant contributor to ultrafine particle growth throughout the continental boundary layer. However, there are uncertainties regarding SOA and its contribution to ultrafine particle growth, and these will be explored in this paper. Additionally, SOA has recently been found to be involved in aerosol nucleation (Metzger et al., 2010), although this will not be a focus of this paper.

There are two important, but uncertain, characteristics of SOA that influence ultrafine particle growth: (1) the amount of SOA formed (or the rate at which it is formed) (Spracklen et al., 2011; Heald et al., 2011) and (2) the condensational behavior of SOA (how SOA condenses to ultrafine particles) (Riipinen et al., 2011; Pierce et al., 2011; Häkkinen et al., 2013; Kuang et al., 2012).

2.1.1 Uncertainty in amount of SOA

Regarding the uncertain amount of SOA, the global budget of SOA is highly unconstrained with bottom-up and top-down estimates ranging from 12 to 1820 Tg (SOA) yr^{-1} (Goldstein and Galbally, 2007; Hallquist et al., 2009; Kanakidou et al., 2005). This uncertainty in the amount of condensing SOA available has important implications on the growth of ultrafine particles as well. Many global models only contain biogenic sources of SOA (and small contributions from anthropogenic SOA) with emissions generally between 10 and 30 Tg yr^{-1} (Pierce et al., 2011; Spracklen et al., 2006; Wainwright et al., 2012), on the low end of the uncertainty range. However, by

comparing GLOMAP global model simulations to aerosol mass spectrometer measurements or organic aerosol mass, Spracklen et al. (2011b) were able to significantly improve the model prediction of organic aerosol mass by adding an additional 100 Tg yr^{-1} of SOA spatially correlated with anthropogenic carbon monoxide (CO) emissions. That additional SOA increases the amount of condensable material in the atmosphere, which increases growth rates of ultrafine particles; however, the extra mass also increases the condensation and coagulation sinks of small particles, which will slow their growth rates and increase their coagulational losses. Thus, it is unclear what overall effect the extra SOA will have on CCN.

2.1.2 Uncertainty in SOA condensational behavior

Regarding the uncertain condensational behavior, many models treat a large fraction of SOA as semi-volatile (average saturation vapor concentration, $C^* \gtrsim 10^{-1}$ μg m^{-3}) and follow the partitioning theory of Pankow (1994) (e.g. Lane and Pandis, 2007). These semi-volatile species reach equilibrium between the particle and gas phases for all particle sizes quickly, which leads to net condensation of SOA proportional to the aerosol mass distribution (Pierce et al., 2011; Riipinen et al., 2011; Donahue et al., 2011). This limit of net condensation of SOA to the mass distribution is called "thermodynamic condensation" by Riipinen et al. (2011) and we will use this terminology here. This causes preferential condensation of the organic mass to particles with $D_p > 100$ nm. This preferential net condensation to accumulation mode particles not only limits the amount of condensation to ultrafine particles, but also enhances the coagulational scavenging of the ultrafine particles by the larger diameter accumulation mode particles. These two factors decrease the survival probability of ultrafine particles and hence can lead to a low influence of nucleation and other ultrafine particles on CCN. However, recent closure studies with field measurements show that observations of nucleation-mode growth can only be explained if a significant fraction of SOA condenses proportional to the Fuchs-corrected aerosol surface area (i.e. diffusion-limited condensation). This suggests that particles of all sizes are not in equilibrium with the vapor phase and that all particles are

undergoing kinetic, gas-phase-diffusion-limited growth (referred to as "kinetic condensation" by Riipinen et al. (2011) and we will use this terminology here). In order for this purely kinetic condensation to occur, the condensing SOA has very low effective volatility ($C^* <\approx 10^{-3}$ μg m^{-3}) created either through gas-phase chemistry, particle-phase chemistry or trapping of semi-volatile species in the particle phase by a semi-solid shell (Donahue et al., 2011; Pierce et al., 2011; Riipinen et al., 2011; Zhang et al., 2012). This kinetic condensation enables condensation of more organic mass to ultrafine aerosols compared to thermodynamic condensation. An important characteristic of this pure kinetic condensation is that all particles in the kinetic regime (diameters smaller than about 50 nm) grow at the same rate (e.g. nm/hr). On the other hand, under thermodynamic condensation, the growth rate scales with $1/D_p$. Thus, under kinetic condensation, ultrafine particles grow more quickly to climatically relevant sizes where they can act as CCN compared to thermodynamic condensation. In summary, thermodynamic condensational behavior assumes that the gas-particle partitioning reaches equilibrium instantly which means that the net particle condensation is proportional to the particle mass. This assumes SOA to be semi-volatile (e.g. $C^* \sim 1$ μg m^{-3}) where the SOA mass reaches thermodynamic equilibrium quickly and partitions into the pre-existing aerosol mass. Kinetic condensational behavior is limited by gas-phase-diffusional growth and thus vapors condense kinetically proportional to the aerosol surface area. This assumes SOA to be effectively non-volatile (e.g. $C^* < 10^{-3}$ μg m^{-3}). This is explored in detail in Riipinen et al., 2011 and Pierce et al., 2011. The reality is somewhere between these two limiting approaches for real compounds with finite saturation vapor pressures, and recent studies have explored this and are discussed in the next section.

2.1.3 Growth rate parameterizations

Two recent studies by Häkkinen et al. (2013) and Kuang et al. (2012) have shown that while particles at most diameters undergo kinetic (surface-area -limited) SOA condensational growth, the smallest (diameters less than 10 or 20 nm) particles do not

grow as fast as the larger particles (see also Manninen et al., 2010; Yli-Juuti et al., 2010). This means that some SOA species are not readily condensing to the smallest particles (likely because of Kelvin effects or Raoult's Law (Pierce et al., 2011)). Häkkinen et al., (2013) used long-term size-dependent growth-rate observations at six sites in Europe and developed a size-dependent growth rate parameterization to slow the growth of the smallest particles during kinetic SOA condensation. The authors found that the growth rate begins to slow for diameters smaller than 7 nm, and that the growth of 1 nm particles due to SOA is approximately 3 times slower than at sizes larger than 7 nm. Furthermore, Häkkinen et al. (2013) also found indications of the importance of non-biogenic SOA in growing freshly formed nanoparticles at the continental sites they investigated (e.g. the anthropogenically influenced SOA from Spracken et al. (2011) and Heald et al. (2011)). In an independent study, Kuang et al. (2012) measured size-dependent growth rates at two field sites to also determine how the growth rate slows for the smallest particles. These authors found that the growth rates were constant down to a diameter of approximately 3 nm, which is a smaller size than found in Häkkinen et al. (2013). Kuang et al. (2012) found that the growth of 1 nm particles due to SOA is approximately 5 times slower than larger particles. It is notable that the studies by Häkkinen et al. (2013) and Kuang et al. (2012) were from different sites and the size ranges investigated were different. These size-dependent corrections to kinetic SOA condensation will influence growth rates and ultrafine particle survival to CCN sizes but have not yet been tested in global aerosol models.

2.2 Methods

In this study we use a global chemical transport model with online aerosol microphysics to test the sensitivity of the simulated aerosol size distributions to (1) the amount of available SOA, (2) SOA condensational methods (i.e. thermodynamic (mass) vs. kinetic (surface area) condensation), as well as (3) two size-dependent nanoparticle growth rate parameterizations that correct for errors due to assuming pure kinetic condensation. We then use global measurements of aerosol size distributions to test the model using various

SOA assumptions. Our goals are to determine the sensitivities of CCN number concentrations to uncertainties in the SOA parameters and determine if we can constrain the parameter uncertainties using the measured size distributions.

2.2.1 Model Description

In this study, we use the global chemical-transport model, GEOS-Chem (www.geos-chem.org), combined with the online aerosol microphysics module, TOMAS (GEOS-Chem-TOMAS) (as described in Pierce et al. (2013)) to test the sensitivity of global aerosol size distributions to SOA condensational behavior, SOA amount, as well as size-dependent growth rate parameterizations. GEOS-Chem-TOMAS uses GEOS-Chem v8.02.02 (www.geos-chem.org) with a 4°x5° horizontal resolution, 30 vertical layers from the surface to 0.01 hPa with meteorological inputs from the GEOS5 reanalysis (http://gmao.gsfc.nasa.gov). GEOS-Chem-TOMAS simulates the aerosol size distribution using 40 size sections ranging from 1 nm to 10 μm. Nucleation rates in all simulations were predicted by ternary homogeneous nucleation of sulfuric acid, ammonia and water based on the parameterization of Napari et al. (2002) scaled down globally by a constant factor of 10^{-5} which has been shown to predict nucleation rates closer to measurements than other commonly used nucleation schemes (Jung et al., 2010; Westervelt et al., 2013). Emissions in GEOS-Chem are described in van Donkelaar et al. (2008). We note that the predicted size distributions and uncertainty ranges in this paper are sensitive to the nucleation scheme, emissions fluxes and size of emitted particles (e.g. Pierce et al. 2009c), but here we explore the modeled partial derivatives to SOA assumptions. Simulations were run for 2001 with one month of spin-up from a pre-spun-up restart file. We test the sensitivity of predicted size distributions to the condensational behavior of SOA in GEOS-Chem-TOMAS by assuming the kinetic and thermodynamic limits of SOA condensation. For thermodynamic condensation, we distribute the SOA across the aerosol sizes proportional to the aerosol mass distribution. For kinetic condensation, we distribute the SOA mass across the aerosol sizes proportional to the

Fuchs-corrected aerosol surface area distribution (Donahue et al., 2011; Pierce et al., 2011; Riipinen et al., 2011).

Traditionally, SOA in GEOS-Chem-TOMAS is formed only from terrestrial biogenic sources, with the biogenic source being a fixed yield of 10% of the monoterpene emissions. This biogenic source of SOA represents an annual flux of 19 Tg (SOA) yr^{-1}. To test the sensitivity of GEOS-Chem-TOMAS to the amount of condensable SOA, we include 100 Tg (SOA) yr^{-1} spatially correlated with anthropogenic CO emissions based on the findings of Spracklen et al. (2011b).

Finally, we test the sensitivity of GEOS-Chem-TOMAS to various nanoparticle size-dependent growth rate parameterizations that correct for deviation from the kinetic SOA condensation limit. The first parameterization implemented into GEOS-Chem-TOMAS is a linear fit based on the findings of Kuang et al. (2012) where the condensation rate of SOA is scaled down from the kinetic limit for particles with D_p of 1 nm to 2.5 nm based on their diameter using the following equation:

$$k = 0.47D_p - 0.18 \quad (1)$$

where k is an empirical unitless condensation scale factor, a linear reduction in the size-dependent mass flux and growth rate (equal to 0.29 for 1 nm particles and 1 for 2.5 nm particles) and D_p is the diameter in nm. Equation 1 was based on Figure 1b from Kuang et al. (2012). The other parameterization that we test in GEOS-Chem-TOMAS is based on the findings of Häkkinen et al. (2013) where a semi-empirical parameterization of condensation-rate scale factors was developed for sub-20 nm particles. This parameterization contains specific growth rates for particles in three diameter ranges (1.5-3 nm, 3-7 nm and 7-20 nm). The growth rates have scaling factors of $k_{1.5\text{-}3nm} = 0.0$, $k_{3\text{-}7nm} = 0.7$ and $k_{7\text{-}20nm} = 1.0$. This set of scaling factors was calculated in Häkkinen et al. (2013) using data from six measurement sites in Europe.

2.2.2 Description of simulations

The various GEOS-Chem-TOMAS simulations in this study are summarized in Table 2.1. The BASE simulations include the biogenic SOA only with an annual flux of 19 Tg (SOA) yr^{-1}. The XSOA simulations include an additional 100 Tg (SOA) yr^{-1} spatially correlated with anthropogenic CO emissions as per Spracklen et al. (2011b). The MASS simulations assume thermodynamic SOA condensation, which condenses to the aerosol size distribution proportional to the aerosol mass via thermodynamic condensation (Pierce et al., 2011; Riipinen et al., 2011; Zhang et al., 2012), while the SURF simulations assume kinetic SOA condensation, which condenses to the aerosol size distribution proportional to the Fuchs-corrected aerosol surface area (Donahue et al., 2011; Pierce et al., 2011; Riipinen et al., 2011; Zhang et al., 2012). The simulations including the linear sub-2.5 nm size dependent growth rate parameterization (corrections to kinetic condensation) based on the findings of Kuang et al. (2012) are labeled with an additional "K". The simulations including the sub-20 nm semi-empirical size dependent growth rate parameterization based on the findings of Häkkinen et al. (2013) are labeled with an additional "H". Note that we only perform size-dependent growth rate simulations with the SURF-XSOA assumptions. This is because the parameterizations are corrections for kinetic condensation (the SURF assumption), and the effect of the K and H parameterizations are stronger under the XSOA simulations.

Table 2.1 Summary of the GEOS-Chem-TOMAS simulations performed in this study.

Simulation name	Condensational Behavior	Additional 100 Tg (SOA) yr^{-1}	Growth rate parameterization based on Kuang et al. (2012)	Growth rate parameterization based on Häkkinen et al. (2013)
MASS-BASE	Thermodynamic (mass)	no	no	no
SURF-BASE	Kinetic (surface area)	no	no	no
MASS-XSOA	Thermodynamic (mass)	yes	no	no
SURF-XSOA	Kinetic (surface area)	yes	no	no
SURF-XSOA-K	Kinetic (surface area)	yes	yes	no
SURF-XSOA-H	Kinetic (surface area)	yes	no	yes

2.2.3 Description of measurements

Surface-based particle size distribution measurements were compiled from the European Supersites for Atmospheric Aerosol Research (www.eusaar.net), from Environment Canada (Pierce et al., 2012; Riipinen et al., 2011; Leaitch et al., 2013), from the RoMANS 2 campaign (instrumentation and site descriptions are same as RoMANS 1 campaign as per Levin et al., 2009), from the BEACHON campaign (Levin et al., 2012) and from Kent State University (Kanawade et al., 2012; Erupe et al., 2010). In this study, 21 ground sites were selected (see Table 2.2 and Figure 2.1) from Europe and North America. At each site, particle size distributions were measured with a Scanning Mobility Particle Sizer (SMPS) (Wang and Flagan, 1990) or a Differential Mobility Particle Sizer (DMPS) (Aalto et al., 2001) instrument. The characteristics of the sites include various terrain types such as coastal, mountain, boreal forest, arctic and rural environments. The air masses measured at each site also vary from polluted to remote continental and marine. However, we have intentionally avoided sites that are located in polluted urban areas as the coarse, 4ºx5º, resolution of the model cannot match these observations. Detailed information on each European site including location and

observed particle number concentrations can be found in Asmi et al. (2011) and Reddington et al., (2011). Information from the North American sites can be found in Pierce et al. (2012), Riipinen et al. (2011), Leaitch et al. (2013), Levin et al. (2009), Levin et al. (2012), Kanawade et al. (2012) and Erupe et al. (2010).

Table 2.2 Summary of surface observation sites used in this study compiled from the European Supersites for Atmospheric Aerosol Research (www.eusaar.net), from Environment Canada (Pierce et al., 2012; Riipinen et al., 2011), from the RoMANS 2 campaign (Levin et al., 2009), from the BEACHON campaign (Levin et al., 2012) and from Kent State University (Kanawade et al., 2012; Erupe et al., 2010). This summary is based on a similar surface observation site summary from Reddington et al. (2011). All date ranges are for one complete year except Kent, Ohio, which is averaged over two years of measurements.

Site name	Elevation(m.a.s.l.)	Aerosol instrument	Year	Recorded Bin Size Range (nm)
Alert, Canada	200	SMPS	2012	10.4 – 469.8
Aspvreten, Sweden	30	DMPS	2005	11.1 – 417.8
Cabauw, Netherlands	60	SMPS	2008	9.4 – 516.0
Egbert, Canada	264	SMPS	2007	10.7 – 392.4
Finokalia, Greece	250	SMPS	2009	11.6 – 916.0
Hohenpiessenberg , Germany	980	SMPS	1999	3.0 – 678.4
Hyytiälä, Finland	181	DMPS	2001	3.2 – 501.0
JRC-Ispra, Italy	209	DMPS	2008	10.0 – 600.0
K-puszta, Hungary	125	SMPS	2006	5.6 – 1000.0
Kent, USA	320	SMPS	2008-2009	3.2 – 914.0
Košetice, Czech Republic	534	SMPS	2009	9.5 – 908.8
Mace Head, Ireland	5	SMPS	2008	8.3 – 467.5
Manitou Experimental Forest, USA	2300	DMPS	2010	15.6 – 354.3
Melpitz, Germany	87	DMPS	2004	3.0 – 802.1
Monte Cimone, Italy	2165	DMPS	2007	4.7 – 466.8
Pallas, Finland	560	DMPS	2001	7.4 – 494.2
Puy de Dôme, France	1465	SMPS	2007	3.0 – 995.0
Rocky Mountain National Park (RMNP), USA	2750	DMPS	2008	32.4 – 22909.0
Schauinsland, Germany	1205	SMPS	2008	10.0 – 800.0
Whistler, Canada	2182	SMPS	2011	14.1 – 572.5
Zeppelin Mountain, Svalbard Islands	474	DMPS	2001	20.1 – 635.1

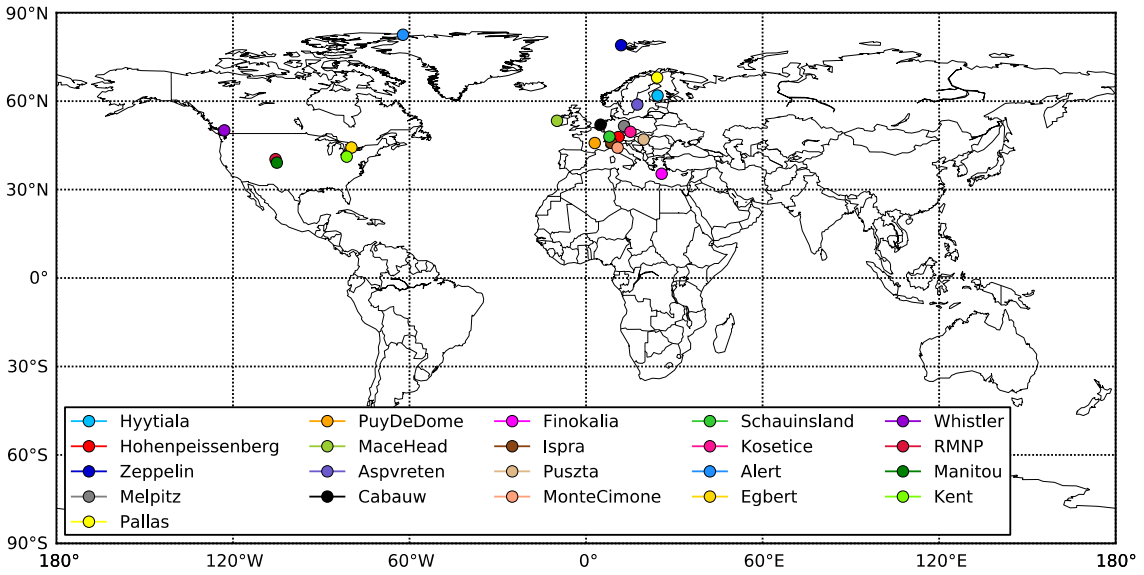

Figure 2.1 Locations of the surface-based measurement sites used in this study.

2.2.4 Numerical analysis of annual-mean size distributions

We evaluate the quality of the model predictions by comparing the predicted, time-averaged aerosol number concentrations with various size cutoffs (e.g. the number concentration of particles with diameters larger than 10, 40, 80 and 150 nm [N10, N40, N80 and N150]) in the grid box and model level of each observational site to the time-averaged number concentration values of the observations. We time-average the model values over the months where measurements were taken. We only perform the time-average spatial analysis and do not perform a time-dependent analysis as our simulations do not necessarily correspond to the same year as the observations. We calculate three metrics to evaluate the model performance. The first is the log-mean bias (LMB) statistic:

$$LMB = \frac{\sum_i (\log_{10}(S_i) - \log_{10}(O_i))}{N} \quad (2)$$

where S_i and O_i are simulated and observed particle number concentrations, respectively for each ground site, i, and N is the number of sites. A LMB of 1 means that the model overestimates, on average, by a factor of $10^1 = 10$, and a LMB of -2 means that the model underestimates, on average, by a factor of $10^{-2} = 0.01$. The other two statistics are the correlation coefficient (R^2) and the slope of the log-log regression (m). The LMB, slope of the linear regression (m) and coefficient of determination (R^2) for each ground site, i, and simulation are plotted in Figure 10 and summarized in Table 2.3.

Table 2.3 Summary of the log-mean bias (LMB), slope of the linear regression (m) and correlation (R^2) for the different simulations. These statistics are found by comparing the annual-average values of the aerosol number concentrations across all sites. Bolded numbers represent the best statistical result between all simulations.

Simulation	LMB				*m*				R^2			
	N10	N40	N80	N150	N10	N40	N80	N150	N10	N40	N80	N150
MASS-BASE	0.203	-0.047	-0.099	-0.199	1.031	0.825	0.729	0.628	0.91	0.90	0.86	0.80
SURF-BASE	0.203	**-0.035**	-0.083	-0.181	1.025	0.827	0.732	0.633	0.91	0.90	0.86	0.80
MASS-XSOA	0.100	-0.067	-0.084	-0.107	**1.003**	0.857	0.783	0.722	**0.92**	**0.91**	0.86	0.80
SURF-XSOA	**-0.030**	-0.052	**0.005**	**0.071**	0.888	**0.876**	**0.859**	**0.852**	0.89	**0.91**	**0.87**	**0.82**

2.3 Results

Figure 2.2 shows the base-case global annual-mean boundary-layer (BL) total number concentration of particles N3, N10, N40 and N80 (the total number concentration of particles with diameter larger than 3 nm, 10 nm, 40 nm and 80 nm respectively) when assuming semi-volatile SOA with condensation proportional to the aerosol mass distribution (MASS-BASE). This figure may be used as a basis for the comparison figures that follow. In this study, we will focus on the BL sensitivities since this is where the observations (with several exceptions) are located and also where the sensitivities of the size distribution to SOA are the highest.

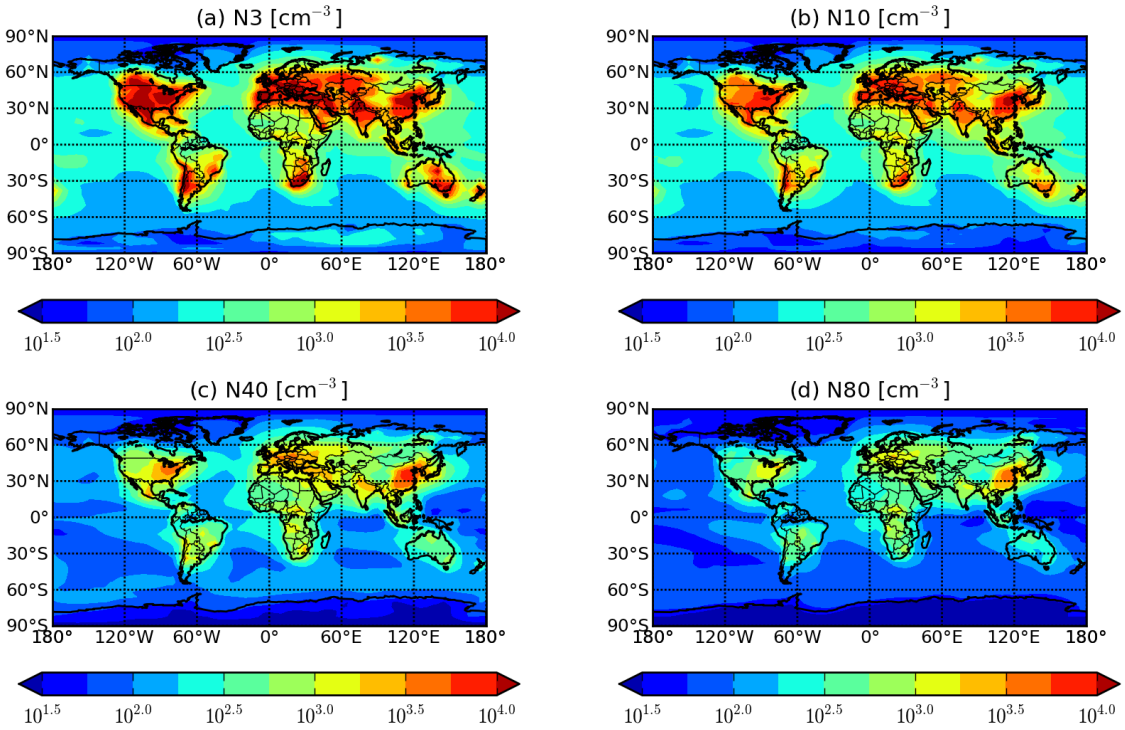

Figure 2.2 Global annual-mean boundary-layer total number of particles (a) N3, (b) N10, (c) N40 and (d) N80 (the total number of particles with diameter larger than 3 nm, 10 nm, 40 nm and 80 nm respectively) for the MASS-BASE case.

2.3.1 Sensitivity to SOA amount

Figure 2.3 shows the global annual-mean percent changes in N3, N10, N40 and N80 throughout the BL between the simulation including an additional 100 Tg (SOA) yr^{-1} correlated with anthropogenic CO emissions (SURF-XSOA) and the SURF-BASE case, both assuming non-volatile SOA (red denotes higher concentrations in the SURF-XSOA simulation). There was a global change of -50.9%, -26.6%, 13.7% and 29.9% in N3, N10, N40 and N80 respectively throughout the BL. The decreases in N3 and N10 due to the extra SOA occur throughout most of the northern hemisphere and through the mid-latitudes of the southern hemisphere. The decreases in N3 are more than 70% throughout much of the globe. N40 and N80 show large increases due to the SOA in anthropogenic CO-source regions (over 100% increases in some regions), but smaller decreases downwind of these regions.

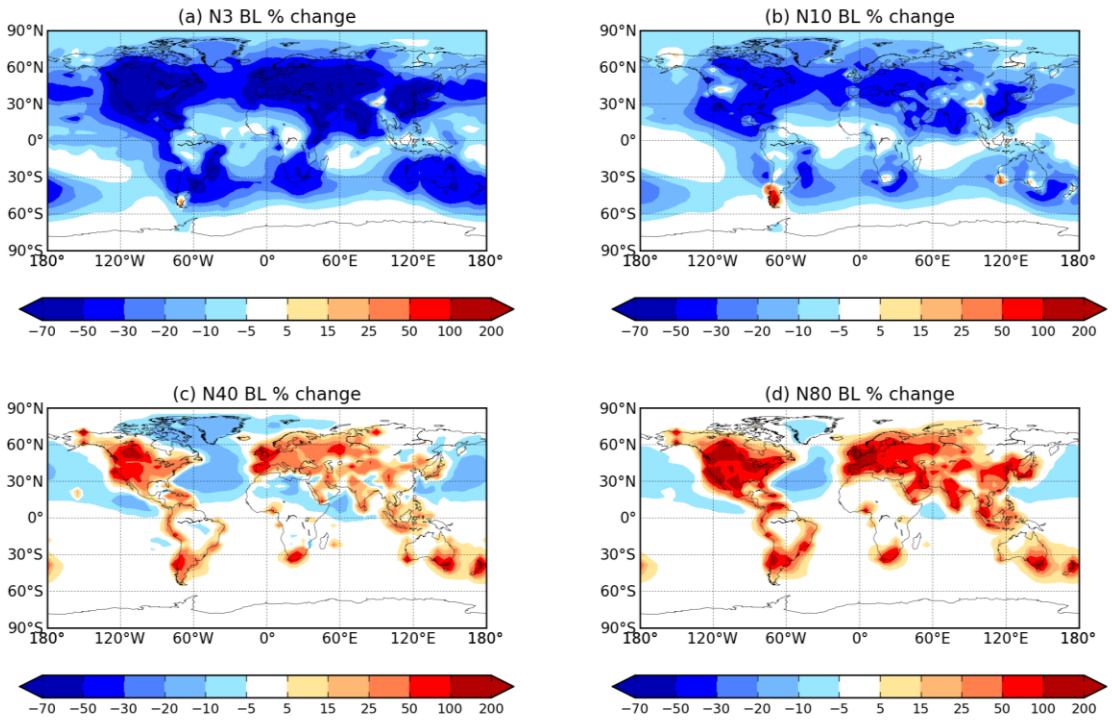

Figure 2.3. Global annual-mean BL changes in (a) N3, (b) N10, (c) N40 and (d) N80 between SURF-BASE and SURF-XSOA (red denotes higher concentrations in the SURF-XSOA simulation). The inclusion of an additional 100 Tg (SOA) yr^{-1} spatially correlated with anthropogenic CO emissions (Spracklen et al., 2011b) caused global decreases in N3 and N10 of 50.9% and 26.6% respectively, however global increases of 13.7% and 29.9% in N40 and N80 respectively.

These increases and decreases are explained through a series of microphysical feedbacks. In anthropogenic CO source regions, there is a large increase in the amount of condensable SOA. This extra SOA grows more ultrafine particles to sizes larger than 40 and 80 nm, thus causing the increase in N40 and N80 in the source regions in the SURF-XSOA case. However, this increase in the number of larger particles increases the condensation and coagulation sinks. This increase in the condensation sink is confirmed in Figure 2.4 where the global annual-mean percent change in sulfuric acid vapor concentration between the same two cases is shown. There is a global decrease in

sulfuric acid vapor of 18.8% (larger near many anthropogenic CO source regions) with the inclusion of the additional SOA since the condensation of sulfuric acid vapor increases with the increased number of large particles (increased condensation sink). The decrease in sulfuric acid causes a suppression of nucleation. Additionally, the increase in coagulational scavenging due to the increased coagulation sink of small particles further decreases the N3 and N10. However, as the air masses move away from the anthropogenic CO source regions, the CCN-sized (N40 and N80) particles are lost by wet deposition more quickly than the smaller particles. In the SURF-BASE simulation (without the extra SOA), there are ultrafine particles that grow to CCN sizes and replace the lost N40 and N80; however, the SURF-XSOA simulation (with the extra SOA) has significantly fewer ultrafine particles to replace the lost N40 and N80. Thus, the SURF-XSOA simulation has lower N40 and N80 concentrations over regions downwind of anthropogenic CO source regions (e.g. the North Atlantic and North Pacific oceans).

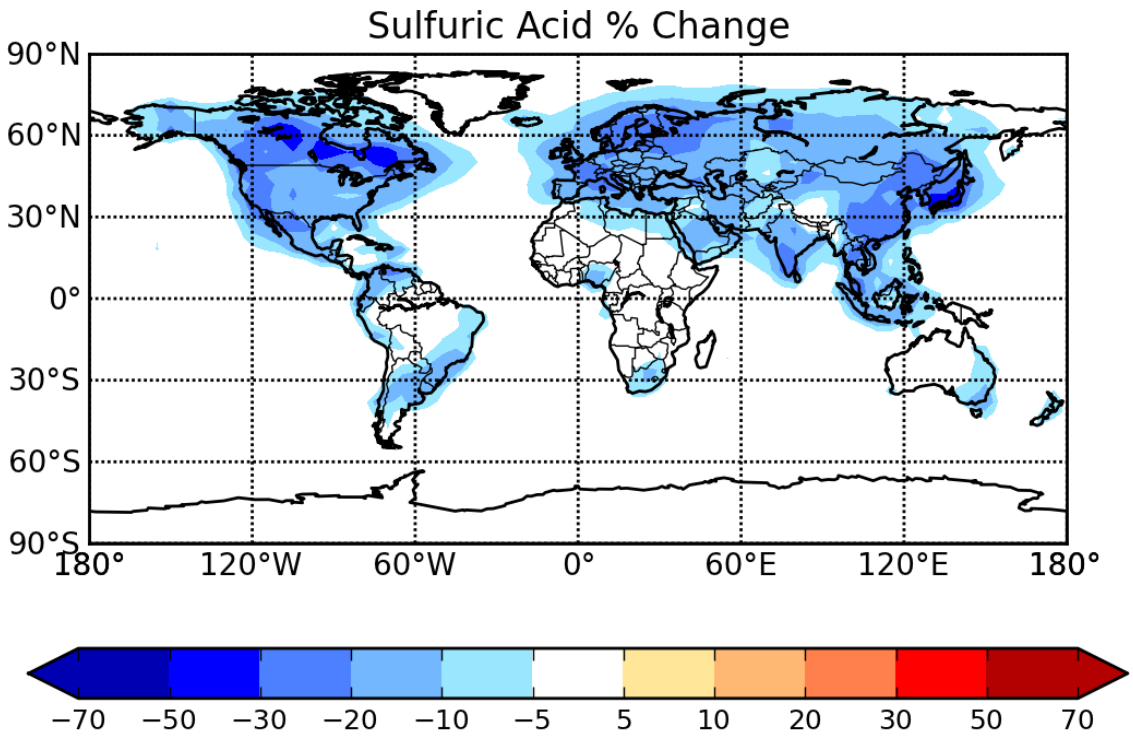

Figure 2.4. Global annual-mean BL changes in sulfuric acid vapor concentration between SURF-BASE and SURF-XSOA. A global BL decrease of 18.8% was observed with the addition of an extra 100 Tg (SOA) yr^{-1} spatially correlated with anthropogenic CO emissions (Spracklen et al., 2011b).

2.3.2 Sensitivity to SOA condensational behavior

Figure 2.5 shows the annual-average percent change in N3, N10, N40 and N80 throughout the BL when switching from thermodynamic SOA condensation to kinetic SOA condensation under the biogenic-only SOA conditions (SURF-BASE – MASS-BASE). There was a global increase of 0.3%, 5.2%, 10.8% and 8.7% in N3, N10, N40 and N80, respectively throughout the BL, due to the SOA condensing more favorably to the ultrafine particles in the SURF-BASE simulation with the kinetic SOA condensation. In some regions downwind of biogenically active regions, N3 decreases by more than 10%. The increased ultrafine particle growth in the biogenically active regions causes an increase in the coagulational sink for small particles and they are removed more quickly, therefore causing a deficiency in N3. As the air masses move over oceanic regions away from these regions, relatively few emitted or nucleated ultrafine particles are available to replace the lost N3. However, in many biogenically active regions, the increases in N40 and N80 (which we use in this study as a proxy for CCN) surpassed 15%, and in the continental tropics the increase exceeded 100%. Therefore, the predicted CCN concentrations are sensitive to the condensational behavior of SOA, consistent with the findings of Riipinen et al. (2011). As field studies (e.g. Riipinen et al. (2011), Pierce et al. (2011) and Pierce et al, (2012)) have found that SOA condensation appears to be closer to the kinetic limit, the higher CCN values in the SURF-BASE simulation may be more appropriate, and we will evaluate this later.

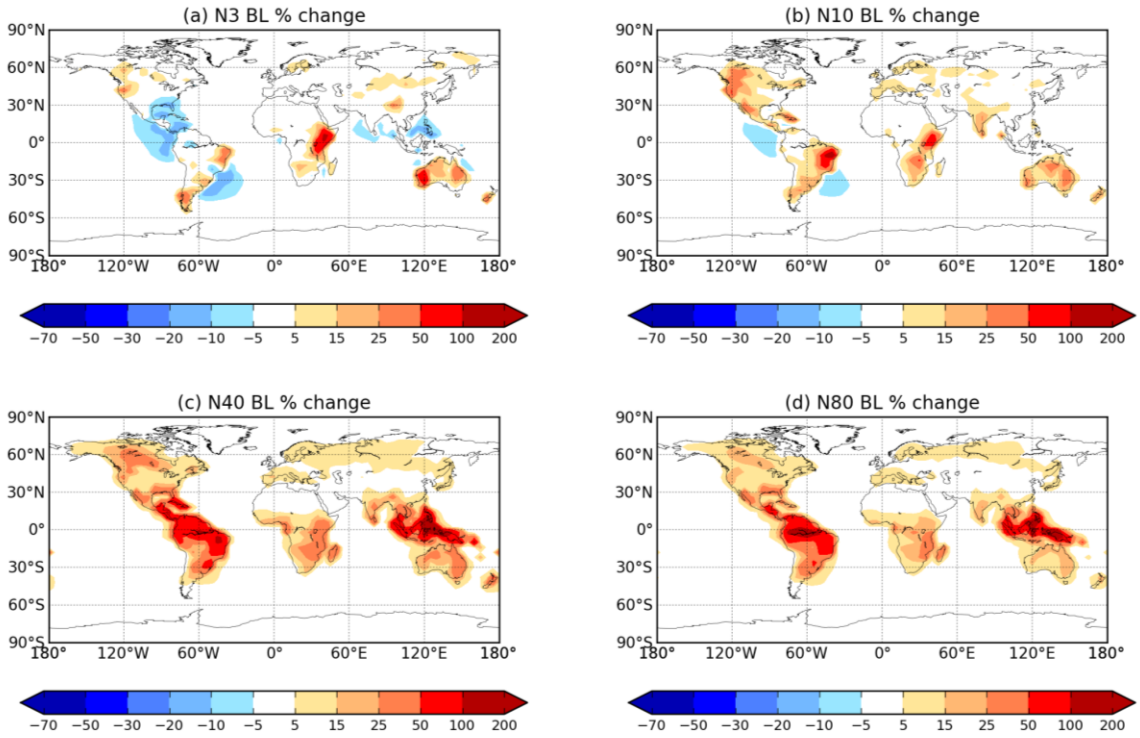

Figure 2.5. Global annual-mean boundary-layer changes in (a) N3, (b) N10, (c) N40 and (d) N80 between MASS-BASE and SURF-BASE (red denotes higher concentrations in the SURF-BASE simulation). There was a global BL increase of 0.3%, 5.2%, 10.8% and 8.7% in N3, N10, N40 and N80 respectively when assuming kinetic condensation. Regions which are biogenically active indicate increases greater than 50% in N40 and N80.

2.3.3 Sensitivity to size-dependent growth rate parameterizations

2.3.3.1 Sub-3 nm growth rate parameterization

Figure 2.6 shows the global annual-mean percent changes in N3, N10, N40 and N80 throughout the BL assuming kinetic SOA condensation, the inclusion of the additional 100 Tg (SOA) yr^{-1} as well as the implementation of the sub-2.5 nm growth rate correction to the kinetic condensation assumption based on the findings of Kuang et al. (2012) (SURF-XSOA-K) from the SURF-XSOA case (red denotes higher concentrations in the SURF-XSOA-K simulation). There was a global change of -0.20%, -0.21%, -0.03% and -0.01% in N3, N10, N40 and N80 throughout the BL respectively. This reduction in number concentrations is due to the decrease in the growth rate of sub-2.5 nm particles

and hence a slight increase in the coagulational scavenging of these nanoparticles before they can grow via condensation. In some regions, there was a decrease in N3 and N10 of greater than 5%, however with this change in the growth rates of the sub-2.5 nm particles, there is negligible change to N40 or N80. This negligible change to CCN sized particles shows that a small change in sub-2.5 nm nucleation mode growth rates is dampened by the effects of aerosol microphysics (nucleation, condensation, coagulation and other processes that shape the aerosol number, size and composition).

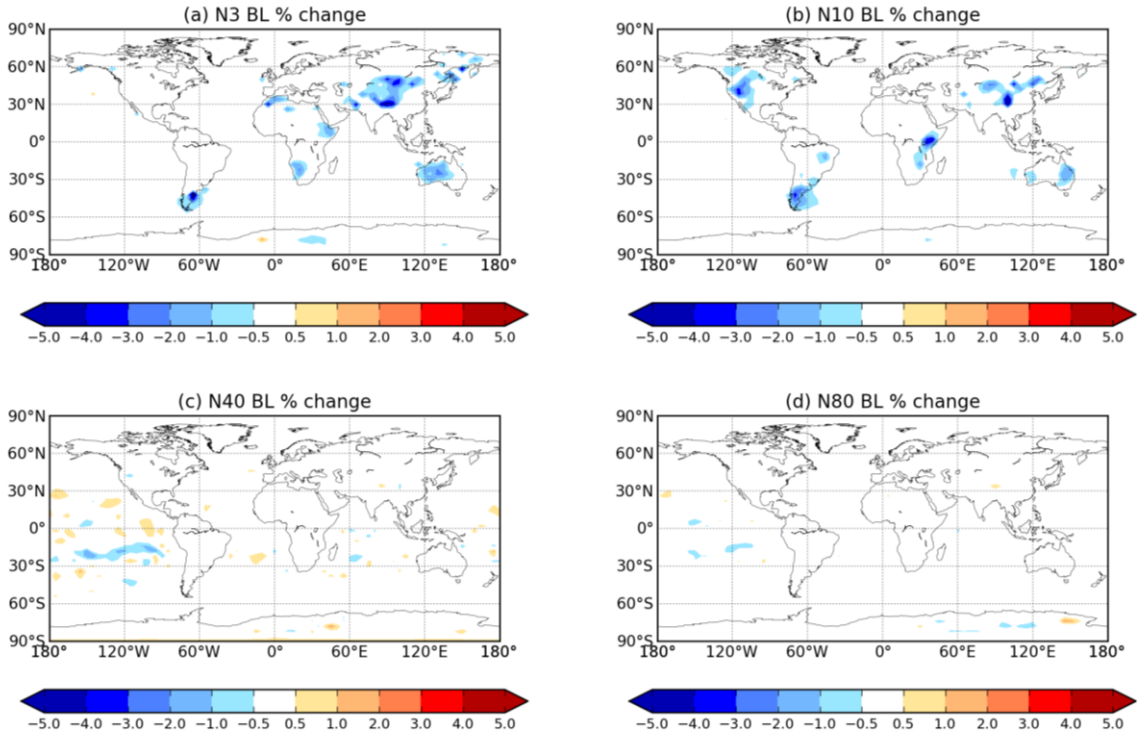

Figure 2.6. Global annual-mean BL changes in (a) N3, (b) N10, (c) N40 and (d) N80 between SURF-XSOA and SURF-XSOA-K (red denotes higher concentrations in the SURF-XSOA-K simulation). There was a global BL decrease of 0.20%, 0.21%, 0.03% and 0.01% in N3, N10, N40 and N80 respectively when the linear sub-2.5 nm growth rate parameterization was included (Kuang et al., 2012).

2.3.3.2 Sub-20 nm growth rate parameterization

Figure 2.7 shows the global annual-mean percent changes in N3, N10, N40 and N80 throughout the BL assuming kinetic SOA condensation, the inclusion of the additional 100 Tg (SOA) yr^{-1} as well as the inclusion of the semi-empirical sub-20 nm growth rate correction to the kinetic condensation assumption based on the findings of Häkkinen et al. (2013) (SURF-XSOA-H) from the SURF-XSOA case (red denotes higher concentrations in the SURF-XSOA-H simulation). There was a global change of -5.8%, -4.4%, -1.0% and -0.6% in N3, N10, N40 and N80 throughout the BL respectively. In some regions, there is a decrease in N3 and N10 of greater than 50%. This semi-empirical size-dependent growth rate parameterization has a much greater effect on global particle number concentrations than the linear sub-2.5 nm growth rate parameterization based on Kuang et al. (2012); however, even with non-negligible decreases in N3 and N10, the effect on global CCN concentrations remains small except for over some continental source regions. The sensitivity of N40 and N80 to changes in growth rates of sub-20 nm particles has been shown to be highly dampened due to other microphysical processes and the effects are much smaller than the other SOA assumptions tested earlier.

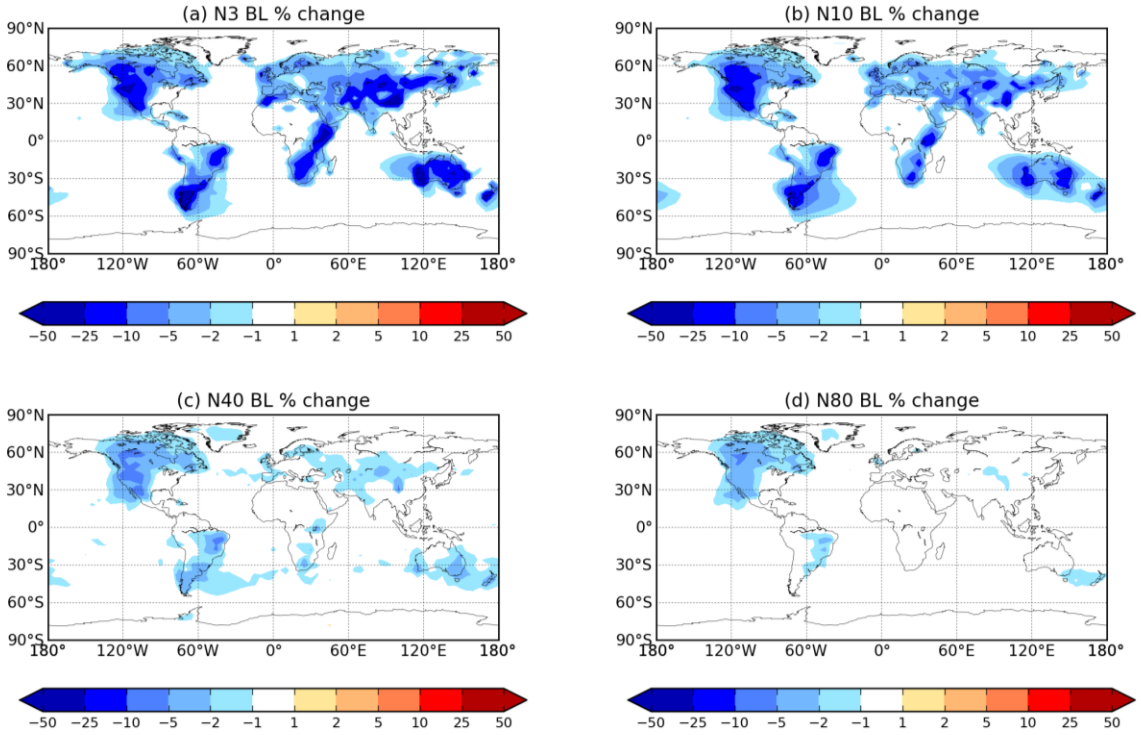

Figure 2.7. Global annual-mean BL changes in (a) N3, (b) N10, (c) N40 and (d) N80 between SURF-XSOA and SURF-XSOA-H (red denotes higher concentrations in the SURF-XSOA-H simulation). There was a global BL decrease of 5.8%, 4.4%, 1.0% and 0.6% in N3, N10, N40 and N80 respectively when the semi-empirical sub-20 nm growth rate parameterization was included (Häkkinen et al., 2013).

2.3.4 Analysis of annual-mean model-measurement comparisons

Figure 2.8 shows the observed and simulated annual- or campaign-mean particle number size distributions for all of the locations outlined in Table 2.2. Included are the MASS-BASE, SURF-BASE, MASS-XSOA and SURF-XSOA cases. The two cases with sub-20 nm growth rate parameterizations (SURF-XSOA-K and SURF-XSOA-H) had small changes from the SURF-XSOA case and thus were not included here. The base-case simulations with biogenic SOA emissions only (MASS-BASE and SURF-BASE), overestimate the number of particles in the nucleation mode and lower-Aitken mode (D_p < 10 nm) and underestimate the number of CCN sized particles (D_p > 40 nm) when compared to measurements at nearly every site. However, with the addition of the 100

Tg (SOA) yr^{-1} (MASS-XSOA and SURF-XSOA), the increase in condensable material causes growth and removal of the ultrafine particles and hence shift the aerosol size distributions towards increasing CCN-sized particles and reducing the numbers of ultrafine particles (as described in section 2.3.1).

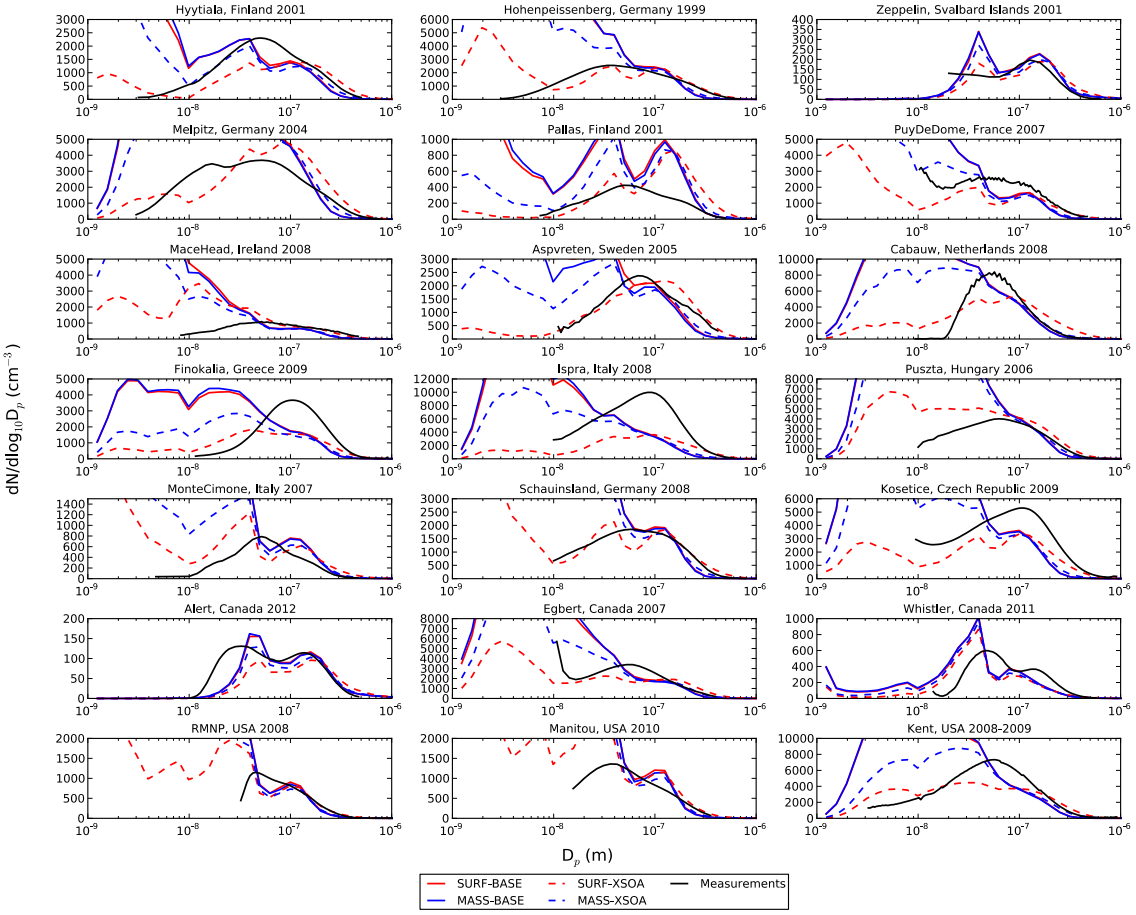

Figure 2.8. Observed and simulated annual- and campaign-mean particle number size distributions for the global sites outlined in Table 2.2. The simulations with sub-20 nm growth rate parameterizations (SURF-XSOA-K and SURF-XSOA-H) had small changes from the SURF-XSOA case and were thus withheld from this figure.

To quantitatively compare the annual-mean model-measurement comparisons, we use the statistics described in Section 2.2.4. Figure 2.9 shows 1:1 plots for the measured and simulated annual-mean N10, N40, N80 and N150 for the MASS-BASE, SURF-BASE, MASS-XSOA and SURF-XSOA cases. N150 was included in this figure since

the additional SOA and changes in the condensational behavior of SOA caused significant changes to the number of particles larger than 150 nm. This change in N150 had a large impact on the shape of the size distribution. In contrast, N3 in size distribution shape analysis behaves enough like N10 and with most of the observations starting around 10 nm, N3 was removed from the model-measurement analysis. Similar to Figure 9, the two cases with sub-20 nm growth rate parameterizations (SURF-XSOA-K and SURF-XSOA-H) were withheld from this figure because of their similarity to the SURF-XSOA case. On each panel, the LMB, slope of the linear regression (m) and coefficient of determination (R^2) between each ground site, i, are labeled, and the dashed lines indicate the 5:1 and 1:5 lines. Table 3 summarizes the LMB, slope of the linear regression (m) and coefficient of determination (R^2) between each ground site, i, and simulation mean number concentrations in the BL. Number concentrations for N10 are consistently overestimated in the model, with MASS-BASE and SURF-BASE having the highest overestimations (LMB = 0.203 or a factor of about 1.6 for both simulations). With the additional SOA, the large positive bias in N10 in the simulations was decreased, the MASS-XSOA simulation improved to LMB = 0.100 (or a factor of 1.3). However, with kinetic SOA condensation and the additional SOA in the SURF-XSOA simulation, the bias in N10 improved further to LMB = -0.030 (or a factor of 0.93). The SURF-XSOA simulation with the lowest LMB had a poorer regression slope (0.888 versus ~1 for the others) and nearly identical R^2 (0.89 versus ~0.91) for N10. The reduction in slope is likely related to more-polluted sites having a greater effect from the extra SOA (greater suppression of small particles). However, across the three metrics, it appears the SURF-XSOA case performs the best due to the large reduction of the bias. For number concentrations of N40, which is our proxy for small CCN, all simulations had a very small low bias (magnitude of LMB $\leq$ 0.067). For N40, SURF-XSOA had the best slope and all simulations had equal R^2. For N80, SURF-XSOA has a slight high bias (LMB = 0.005) while the others are biased low by a larger magnitude. SURF-XSOA has the most favorable conditions for the growth of ultrafine particles to larger sizes, and this shows in this metric. SURF-XSOA does significantly better for the slope of N80 than the other simulations while having similar R^2 as the other simulations. SURF-XSOA does even

better for N150 (the number concentration of particles with diameters larger than 150 nm) with a smaller bias, better slope and slightly better R^2 than the other simulations.

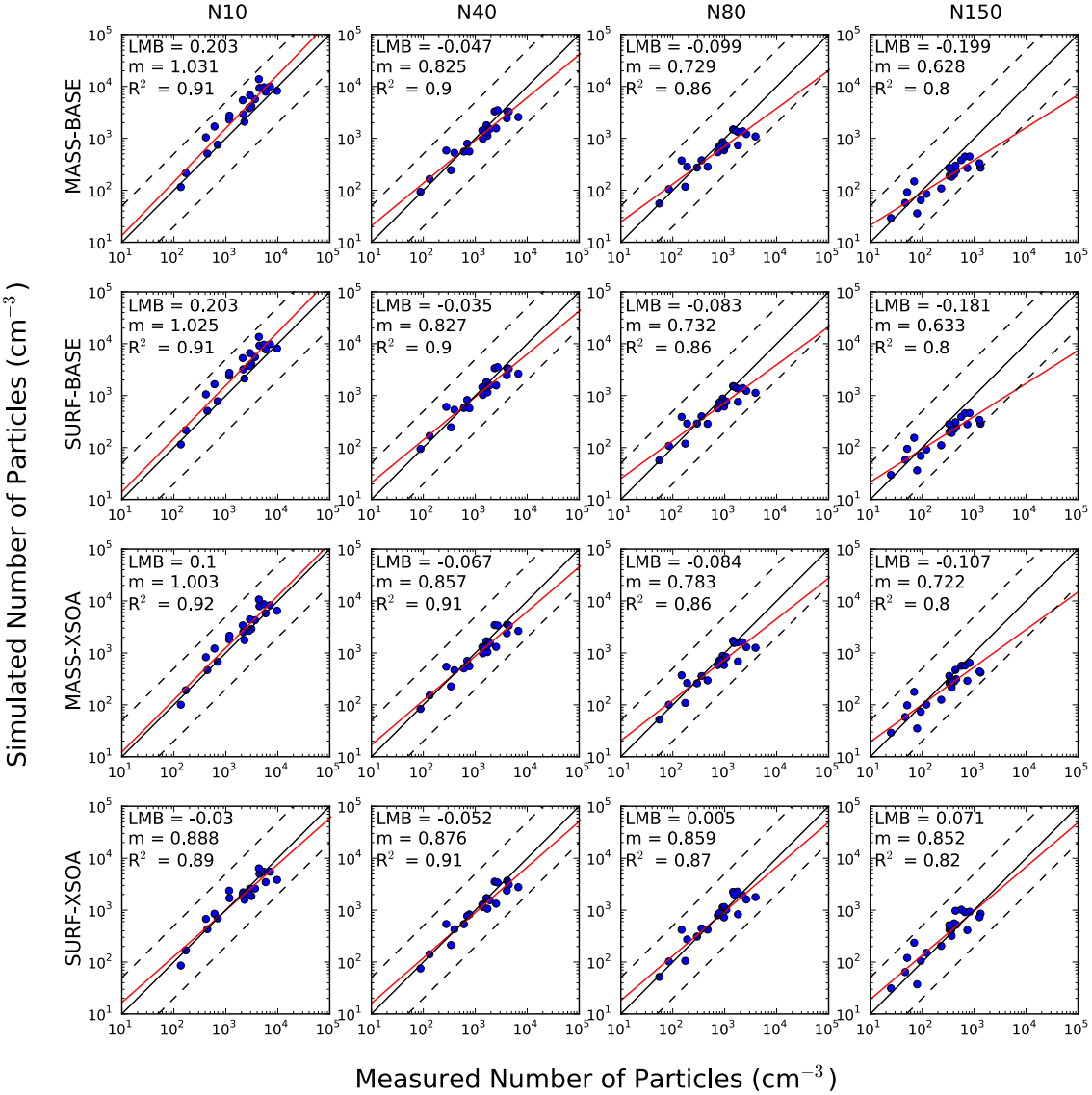

Figure 2.9. 1:1 plots for measured and simulated annual-mean N10, N40, N80 and N150 (the total number of particles with diameter larger than 150 nm), calculated log-mean bias (LMB), slope of the linear regression (m), and correlation (R^2). The dashed black lines indicate 5:1 and 1:5 lines. The simulations with the sub-20 nm growth rate parameterizations (SURF-XSOA-K and SURF-XSOA-H) were withheld from this figure. A summary of the statistics is compiled in Table 2.3.

There is a significant improvement in most metrics when the additional SOA was included (i.e. from MASS-BASE to MASS-XSOA); however, there is also a significant improvement in all metrics when kinetic condensation was assumed instead of thermodynamic condensation (i.e. MASS-BASE to SURF-BASE). This indicates that both the amount and condensational behavior of SOA are important in order to accurately represent size distributions. However, it appears that the SURF-XSOA case generally performs the best with lower biases, better slopes overall, and similar coefficient of determinations (R^2) for all size cutoffs. This conclusion is evidence that kinetic SOA condensation with extra, anthropogenically influenced SOA improves aerosol size distributions in models. However, we must stress that the N10, N40, N80 and N150 could be wrong or right for many reasons other than the SOA assumptions tested here. For example, the size distributions have all been shown to be sensitive to uncertainties to nucleation (Merikanto et al., 2009; Pierce and Adams, 2009c; Reddington et al., 2011; Spracklen et al., 2008; Wang and Penner, 2009), primary emissions (Adams and Seinfeld, 2003; Pierce and Adams, 2006, 2009c; Reddington et al., 2011; Spracklen et al., 2011a), wet/dry deposition (Croft et al., 2012) and other factors (Lee et al., 2013). A recent global model uncertainty study by Lee et al., 2013 finds that the relative uncertainties to global mean CCN number concentrations vary between model parameters. The relative uncertainty to CCN (from -2σ to 2σ) due to accumulation mode dry deposition, Aitken mode dry deposition, anthropogenic SOA emissions, biogenic SOA emissions and boundary layer nucleation are approximately 40%, 18%, 20%, 12% and 5% respectively (Lee et al., 2013). Additionally, the sub-grid-scale variability in the aerosol size distribution that is not resolved within the coarse grid boxes will result in error in our comparisons.

2.4 Conclusions

In this study we have tested the sensitivity of the global aerosol microphysics model GEOS-Chem-TOMAS to the amount and condensational behavior of secondary organic aerosol (SOA) in order to more accurately predict the number concentration of cloud condensation nuclei (CCN) sized particles. The model output was then evaluated against ground-based measurements to test which assumption yielded the most accurate results.

An additional 100 Tg (SOA) yr^{-1} spatially correlated with anthropogenic carbon monoxide (CO) emissions was then added to the model consistent with Spracklen et al. (2011b) and Heald et al. (2011). The addition of the 100 Tg (SOA) yr^{-1} (assumed to be non-volatile) increased global boundary-layer (BL) N40 (particles with D_p > 40nm, our proxy for small-sized CCN in this study) by 13.7% from the biogenic SOA source only simulation.

When assuming low-volatility SOA with condensation proportional to the aerosol mass distribution, or "thermodynamic condensation" as per Riipinen et al. (2011), condensation of SOA was preferential to accumulation mode particles (Pierce et al., 2011; Riipinen et al., 2011). This caused an increase in accumulation and coarse mode particles and an underestimate of N40. The assumption of non-volatile SOA with condensation proportional to the Fuchs-corrected aerosol surface area, or "kinetic condensation" as per Riipinen et al. (2011), caused preferential condensation of SOA to ultrafine particles relative to "thermodynamic condensation" (Donahue et al., 2011; Pierce et al., 2011; Riipinen et al., 2011). This in turn grew ultrafine particles quickly and increased N40. When assuming kinetic condensation, the global change in BL N40 compared to assuming thermodynamic condensation yielded an increase of 10.8%.

Two size-dependent growth rate parameterizations were also implemented. The first parameterization involved the condensation rate of SOA to be scaled down from the kinetic limit for particles with D_p of 1 nm to 2.5 nm based on their diameter with a linear increase in growth rate from 1 to 2.5 nm sized particles as per Kuang et al. (2012). The second parameterization included semi-empirical size-dependent growth rate factors for three ranges of particles of sizes 1.5 nm to 20 nm as per Häkkinen et al. (2013). The sub-

2.5 nm growth rate parameterization based on Kuang et al. (2012) yielded a -0.03% global change in BL N40. The sub-20 nm semi-empirical growth rate parameterization from Häkkinen et al. (2013) yielded a -1.0% global change in BL N40, however there were regions with decreases in BL N40 greater than 50%. The global BL effects of these growth rate parameterizations, however, are within other uncertainties in the model as discussed in section 2.3.4.

From statistical analysis, the assumption of kinetic condensation of SOA combined with the additional SOA spatially correlated with anthropogenic CO emissions performed the best across measurement sites for nearly all statistical metrics. However, the spatial resolution of this version of GEOS-Chem-TOMAS is much too large to resolve specific site characteristics. Therefore, it is expected that with grid boxes on the order of hundreds of kilometers, it may be difficult and impractical to tune the model on a site-specific basis.

While metrics such as primary emission, nucleation schemes and deposition all carry significant errors, this study has shown the importance of various assumptions regarding organic aerosol (amount and condensational behavior of SOA) in global microphysics models, and the influence that SOA can have on global particle size distributions. It is therefore important that these factors are appropriately included in order to provide further insights into the effect of organic aerosol on climatically relevant particles. Future studies could use size-resolved composition from state of the art instruments to further constrain SOA; it is important to not only get the size distribution correct, but it is important to get the composition correct too. More sophisticated SOA schemes involving SOA volatility and chemistry may further improve size distributions; however, combining these SOA schemes with aerosol microphysics is computationally expensive. Additionally, because SOA is also involved in aerosol nucleation (Metzger et al., 2010), the uncertainties in CCN due to SOA presented here are likely underestimated; however, a recent study (Scott et al., 2013) shows that uncertainties in CCN due to the SOA contribution to growth are greater than that of the SOA contribution to nucleation.

CHAPTER 3

AEROSOL SIZE DISTRIBUTION RESPONSE TO ANTHROPOGENICALLY DRIVEN HISTORICAL CHANGES IN BIOGENIC SECONDARY ORGANIC AEROSOL FORMATION *

* D'Andrea, S. D., Acosta Navarro, J. C., Farina, S., Riipinen, I., Pierce, J. R.: Aerosol size distribution response to anthropogenically driven historical changes in biogenic secondary organic aerosol formation, in preparation for Atmospheric Chemistry and Physics, 2013.

3.1 Introduction

The Earth's radiation balance is directly affected by aerosol particles by absorption, scattering and reflection of solar radiation (Rosenfeld et al., 2008; Clement et al., 2009) as well as indirectly affected by aerosols by alteration of cloud properties and lifetimes (Charlson et al., 1992). The uncertainty associated with aerosol radiative forcing, particularly the indirect effect, is a large source of uncertainty in global climate models (Solomon et al., 2007). However, the influence of aerosols on cloud droplet number concentration (CDNC) is driven by the number concentration of cloud condensation nuclei (CCN), or the particles on which cloud droplets form. The number concentration of CCN is highly dependent on the aerosol size distribution (Dusek et al., 2006; McFiggans et al., 2006; Petters and Kriedenweis, 2007; Pierce and Adams, 2007), therefore the size-dependent number of all sizes of particles must be accurately represented to simulate CCN number concentrations correctly.

The two dominant sources of aerosol number to the atmosphere are formation of new particles (diameter ~1 nm) via nucleation (Kulmala et al., 2004) or primary emissions (Putaud et al., 2004; Stanier et al., 2004). In order for freshly nucleated or

emitted nanoparticles to influence atmospheric CCN number concentrations, they must undergo condensational growth (Pierce and Adams, 2007; Vehkamäki and Riipinen, 2012). However, the survival probability of nanoparticles depends on the competition between condensational growth and coagulational scavenging with pre-existing aerosol (Kerminen and Kulmala, 2002; Pierce and Adams, 2007; Kuang et al., 2009; Westervelt et al., 2013).

The growth of particles to CCN sizes due to condensation of sulfuric acid is well known (Sipilä et al., 2010), however the condensation of low-volatility organic aerosols (OA) have also recently been shown to play a substantial role in particle growth (Kerminen et al., 2012; Riipinen et al., 2011; Carslaw et al., 2010; Makkonen et al., 2012). Measurements of the submicron particle composition throughout the continental boundary layer show 20 – 90% of the total mass to be OA (Jimenez et al., 2009). OA enter the atmosphere through primary biogenic emissions as well as by anthropogenic emission sources such as vehicles or residential heating (Hallquist et al., 2009). Based on analysis of measurement data at numerous locations in the Northern Hemisphere, oxygenated OA comprises between 63 and 95% of the total OA and is a known precursor for secondary organic aerosol (SOA) (Zhang et al., 2007; Ng et al., 2010; Zhang et al., 2011). Volatile organic compounds (VOCs), biological volatile organic compounds (BVOCs) and intermediate volatile organic compounds have also been shown to be precursors for SOA (Donahue et al., 2009; Hallquist et al., 2009). SOA formation occurs when gas phase, aerosol-phase and cloud-phase chemical processes involving volatile organic compounds form products with low enough volatility to remain in the condensed phase (Hallquist et al., 2009; Wang et al., 2010; Lim et al., 2010). However, it has been observed that in regions where there is mixing of anthropogenic and biogenic emissions, anthropogenic emissions may enhance SOA formation from BVOCs (Carleton et al., 2010; Spracklen et al., 2011, de Gouw et al., 2005). Regardless of the formation mechanism, additional SOA mass to pre-existing aerosol causes a net condensational flux to the aerosol phase. This increased condensational flux can enhance the growth of ultrafine aerosols (Pierce et al., 2011; Riipinen et al., 2011, D'Andrea et al., 2013). Therefore, anthropogenic and BVOC emissions both have a significant impact on SOA

formation, CCN number concentrations and ultimately climate.

BVOCs also play an important role in tropospheric chemistry and pollution by reacting with the hydroxyl radical (OH) and ozone (O_3). Recent studies on historical emissions of BVOCs have shown that BVOC emissions have been affected by anthropogenic influences over the past millennium (Acosta Navarro et al., in prep; Kaplan et al., 2010). Changes in land use, temperature and carbon dioxide (CO_2) concentrations have all had significant impacts on the emissions of BVOCs. A recent model reconstruction of terpenoid BVOC emissions over the past millennium predict changes to three dominant SOA-producing BVOC classes (isoprene, monoterpenes and sesquiterpenes) (Acosta Navarro et al., in prep). They predicted that globally averaged isoprene emissions have decreased over the past millennium due to land-use changes causing a reduction in high isoprene-emitting natural shrubs and broadleaf trees to low emitting crop and grazing land. They also predicted that globally averaged monoterpene and sesquiterpene emissions have increased over the past millennium due mainly to global increases in temperature (the monoterpene- and sesquiterpene-emitting vegetation has not decreased to the same degree as the isoprene-emitting vegetation). However, all three BVOC classes show both increases and decreases in various regions due to competing factors. The most dominant cause of BVOC emission changes has been from anthropogenic factors, where land-use change has had the most dramatic impact by decreasing the isoprene emissions.

In this paper, we use these modeled estimates of the three dominant BVOC classes' emissions from the years 1000 to 1990 to test the influence of anthropogenic changes in BVOC emissions on SOA formation, global aerosol size distributions and CCN to quantify the net impact of these anthropogenic BVOC changes on aerosols. We do not take into account the potential effects of anthropogenic pollution on the yields of biogenic SOA from BVOCs because of the large uncertainties in these enhancements. In the following section, we investigate the global millennial changes in biogenic emissions from Acosta Navarro et al. (in prep). Section 3.3 describes the model used in this study and the methods used for formation of SOA from the biogenic terpenoid emissions. Section 3.4 describes the results, highlighting the global changes in particle size

distributions due to the millennial changes in BVOC emissions, and the climatic implications associated with these changes.

3.2 Emission changes

In this subsection, we highlight the results from Acosta Navarro et al. (in prep), but for more details on, e.g. vegetation maps, see Acosta Navarro et al. (in prep). The historic BVOC emissions in this paper were predicted by using a modeling system that estimates the net emission of gases and aerosols from terrestrial sources into the atmosphere. The modeling system includes emissions-driving variables such as surface air temperature, downward solar radiation at the surface, soil water content, leaf area index, carbon dioxide (CO_2) concentrations, vegetation maps and soil wilting point. Multiple simulations were run with the model to test the sensitivity to the variables aforementioned and a millennial emissions inventory for the three dominant terpenoid BVOC classes was created. This method is described in more detail in section 3.3.2.

3.2.1 Isoprene emission changes

Isoprene has the highest emission rates of the three BVOCs investigated in this study with mean emissions over the period 1000-1990 greater than 100 mg m^{-2} day^{-1} over tropical rainforests (Figure 3.1a) (Acosta Navarro et al., in prep). Isoprene emissions are dominant in tropical and sub-tropical regions but emit much less in boreal regions. Absolute and percent changes in the spatial distribution of mean isoprene from the period 1000-1010 to 1980-1990 are shown in Figure 3.1b and 3.1c respectively. Globally averaged, isoprene emissions over this period decrease by 11% and are due predominantly to cropland expansion and CO_2 concentration effects. The changes in land-use due to natural high isoprene-emitting broadleaf trees and shrubs being converted to low isoprene emitting crops, such as plantations and pastures have directly decreased isoprene emissions by greater than 75% regionally (Figure 3.1c). Large portions of North America, Australia, Eurasia and southern South America show these strong decreases. However, from Figure 3.1b, the absolute change in isoprene emissions in most of the

Northern Hemisphere are negligible due to lower absolute emissions (Figure 3.1a), even though the percent changes in Figure 3.1c suggest otherwise. The tropical and sub-tropical regions with high isoprene emissions are the regions with the largest absolute changes in emission over this time period. Isoprene emissions are also known to decrease with increasing CO_2 concentrations (Peñuelas et al., 2010). Therefore, increasing CO_2 concentrations in the present-day atmosphere also contribute to the decrease in isoprene emissions. However, isoprene emissions in some regions where the natural vegetation has remained unaltered over the past millennium have increased by greater than 50% due to the increase in surface air temperature.

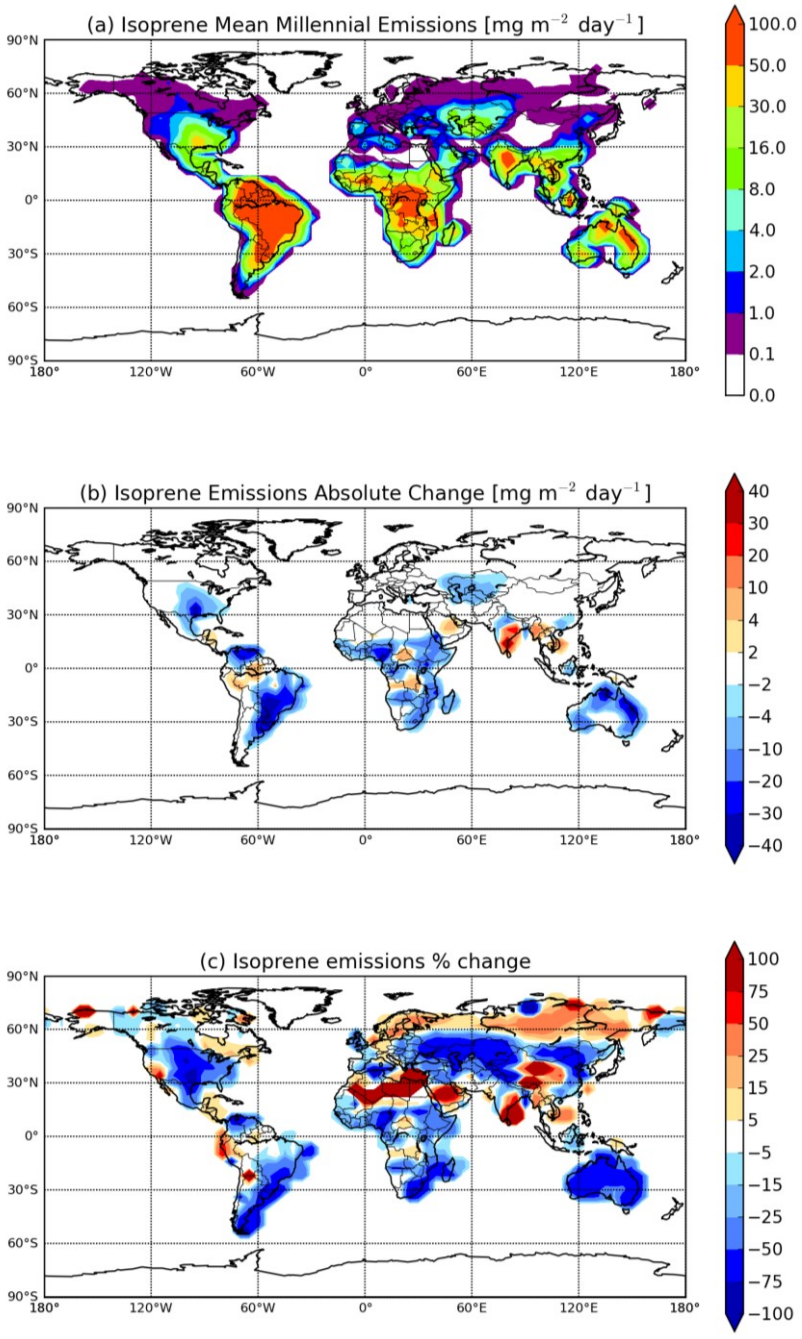

Figure 3.1. (a) Globally averaged millennial isoprene emissions over the years 1000-1990 in mg m^{-2} day^{-1}, (b) absolute change in isoprene emissions between the years 1000-1010 and 1980-1990 in mg m^{-2} day^{-1}, and (c) percent change in isoprene emissions between the years 1000-1010 and 1980-1990. An increase in isoprene emissions is represented by red colors, and a decrease in isoprene emissions by blue in (b) and (c).

3.2.2 Monoterpene emission changes

Along with changes in isoprene emissions over the past millennium, monoterpene emissions have also changed, but overall due to different environmental and anthropogenic influences. Figure 3.2a is a map of globally averaged monoterpene emissions over the years 1000-1990. Mean emissions of monoterpenes over the period 1000-1990 are an order of magnitude lower than isoprene emissions, but are still greater than 10 mg m^{-2} day^{-1} in tropical and sub-tropical regions (Acosta Navarro et al., in prep). Figure 3.2b and 3.2c show the absolute and percent change in monoterpene emissions from pre-industrial (1000-1010) to present-day (1980-1990) respectively. The globally averaged change in monoterpene emissions over this period increase approximately 6%; however, there are regional increases of greater than 75% such as southwestern United States, western Australia and some regions in Asia (red regions). The regions of large increases are predominantly due to colonization and the development of agriculture in regions where monoterpene emitting vegetation was previously scarce. Figure 3.2c suggests large changes in emissions in regions such as the Sahara, northern Canada and northern Asia, but as Figure 3.2b indicates, the absolute changes in emissions in those regions are negligible due to very low emissions. However, in most regions there is an increase in monoterpene emissions of approximately 5-25%. This modest increase in emissions is driven by temperature anomalies and the introduction of vegetation with similar monoterpene emissions as the natural vegetation. There are significant regions of decreasing monoterpene emissions such as central North America, southeastern South American, eastern Australia and central Eurasia (blue regions). The decrease in emissions in these regions is due to strong deforestation and a replacement of natural vegetation with low monoterpene-emitting species.

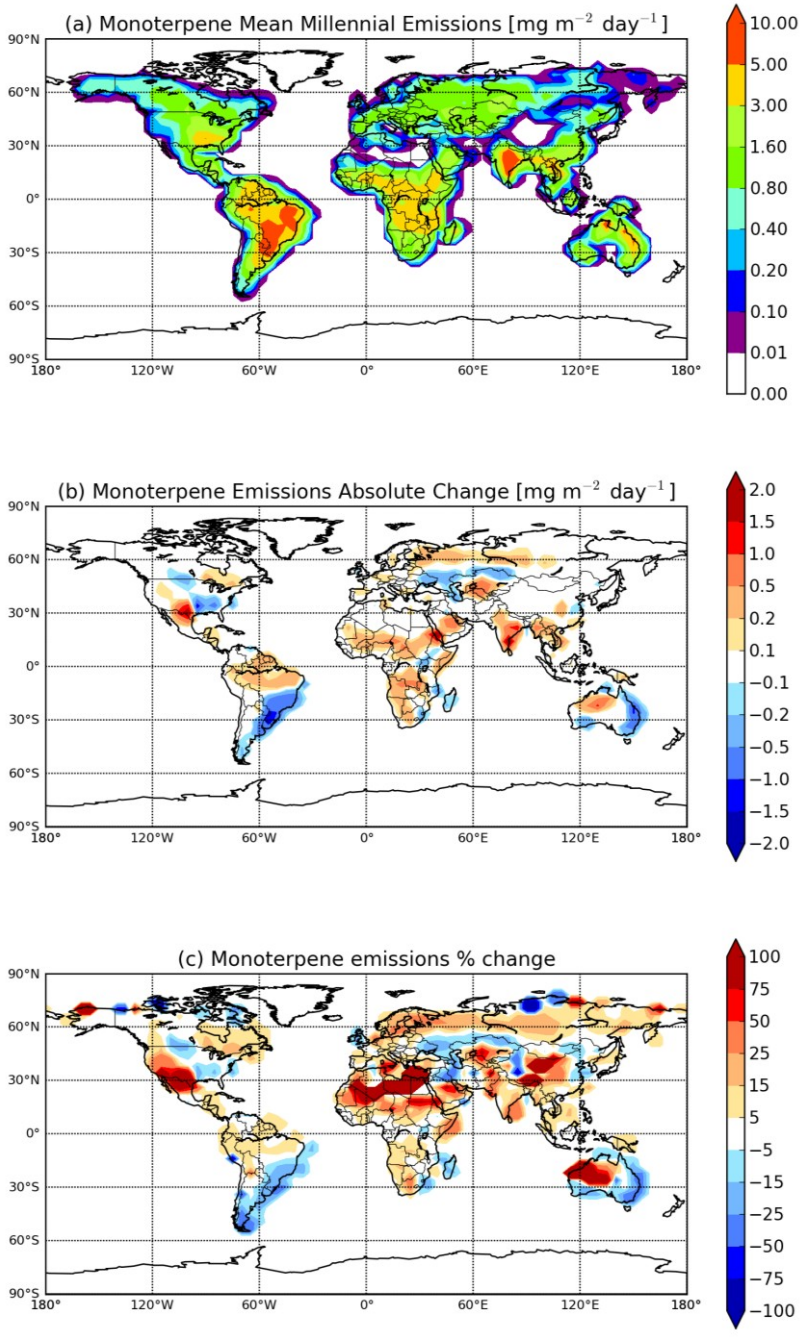

Figure 3.2. (a) Globally averaged millennial monoterpene emissions over the years 1000-1990 in mg m^{-2} day^{-1}, (b) absolute change in monoterpene emissions between the years 1000-1010 and 1980-1990 in mg m^{-2} day^{-1}, and (c) percent change in monoterpene emissions between the years 1000-1010 and 1980-1990. An increase in monoterpene emissions is represented by red colors, and a decrease in monoterpene emissions by blue in (b) and (c).

3.2.3 Sesquiterpene emission changes

Similar to changes in monoterpene emissions over the past millennium, sesquiterpene emissions have also increased. Figure 3.3a is a map of globally averaged sesquiterpene emissions over the years 1000-1990. Mean emissions of sesquiterpenes over the period 1000-1990 are an order of magnitude lower than monoterpene emissions, and two orders of magnitude lower than isoprene emissions. Sesquiterpene emissions exceed 0.5 mg m^{-2} day^{-1} in tropical and sub-tropical regions (Acosta Navarro et al., in prep), and are spatially distributed similar to that of monoterpenes. Figure 3.3c shows the percent change in sesquiterpene emissions from pre-industrial (1000-1010) to present-day (1980-1990). Following the same trend as monoterpenes, the globally averaged change in sesquiterpene emissions over this period increase by approximately 7%; however, there are regional increases of greater than 75% such as southwestern United States, western Australia and some regions in Asia (red regions). The causes of the changes in sesquiterpene emissions are analogous to the changes in monoterpene emissions. The changes are predominantly due to colonization and the development of agriculture in regions where sesquiterpene emitting vegetation was previously limited. Also analogous to monoterpene emissions, Figure 3.3c suggests important changes in sesquiterpene emissions in regions such as the Sahara, central and northern Asia, and northern Canada. This over-exaggeration is similarly due to regions with very low emissions of sesquiterpenes (Figure 3.3a) where the absolute changes in emissions are negligible (Figure 3.3b). However, in all continents except South America, sesquiterpene emissions increase 5-50%. This increase in emissions is mainly driven by temperature anomalies.

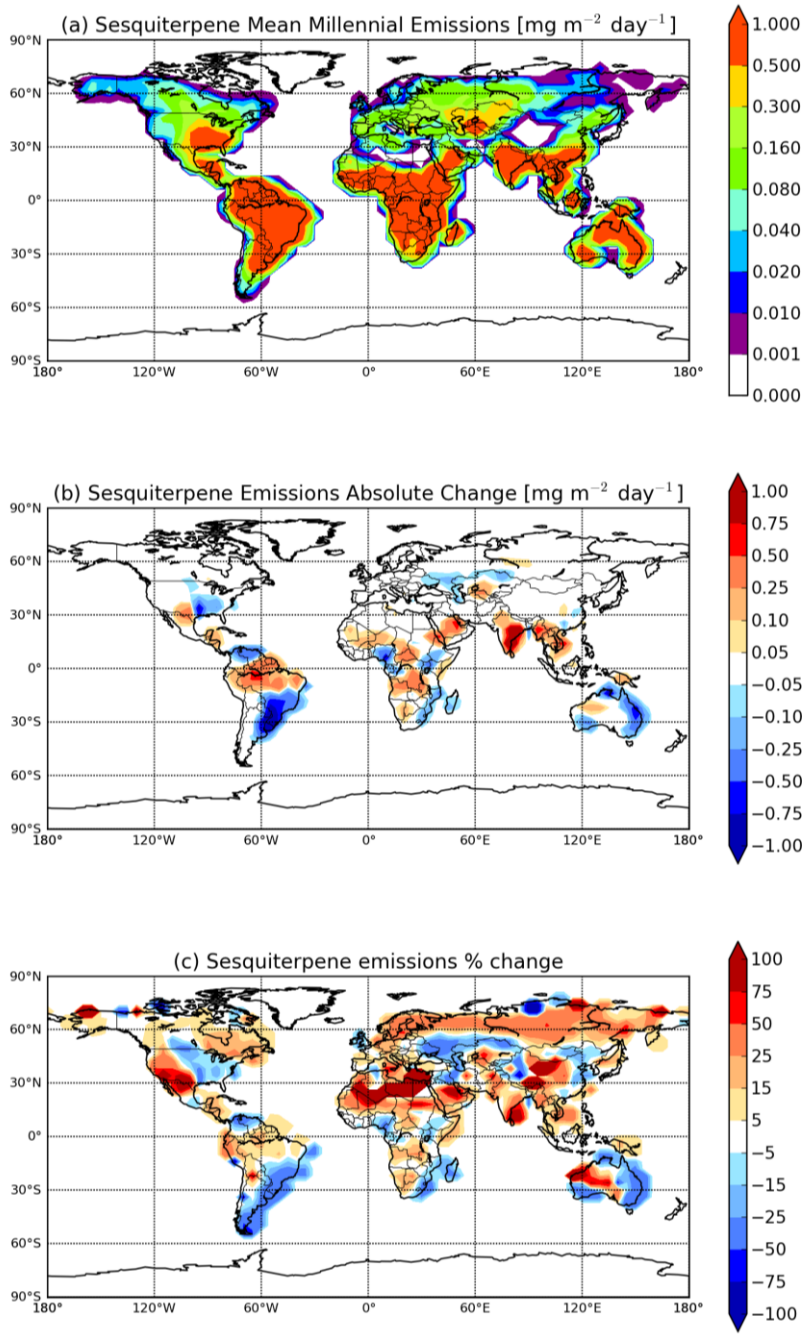

Figure 3.3. (a) Globally averaged millennial sesquiterpene emissions over the years 1000-1990 in mg m^{-2} day^{-1}, (b) absolute change in sesquiterpene emissions between the years 1000-1010 and 1980-1990 in mg m^{-2} day^{-1}, and (c) percent change in sesquiterpene emissions between the years 1000-1010 and 1980-1990. An increase in sesquiterpene emissions is represented by red colors, and a decrease in sesquiterpene emissions by blue in (b) and (c).

Figure 3.4 shows globally averaged isoprene (blue), monoterpene (red) and sesquiterpene (green) emissions over the time period 1000-1990. Monoterpene and sesquiterpene emissions decrease over the years 1000-1800, and then increase from 1800-1990. From 1000-1800, land-use changes cause the decrease in emissions; however, over the period 1800-1990, increases in CO_2 concentrations and temperature drive the increase in emissions. Therefore, to simulate conditions with the least anthropogenic influence, the decadal-averaged BVOC emissions from 1000-1010 are used to simulate pre-industrial conditions in this study. Decadal trends in emission changes of isoprene, monoterpenes and sesquiterpenes remained reasonably constant relative to each other throughout the period 1000-1800, whereas changes in the three BVOC emissions during the years 1950-1990 drastically differ (Acosta Navarro et al., in prep). From the years 1950-1990, monoterpene and sesquiterpene emissions increase; however, isoprene emissions strongly decrease. Therefore, using decadal-averaged BVOC emissions from 1980-1990 are reasonable representations of present day values. The decadal averaged emissions over the years 1980-1990 are also the most recent, and are the most anthropogenically influenced in the Acosta Navarro et al. (in prep) study. Therefore, this range of years is the most appropriate range to use for present day BVOC emissions in our input dataset.

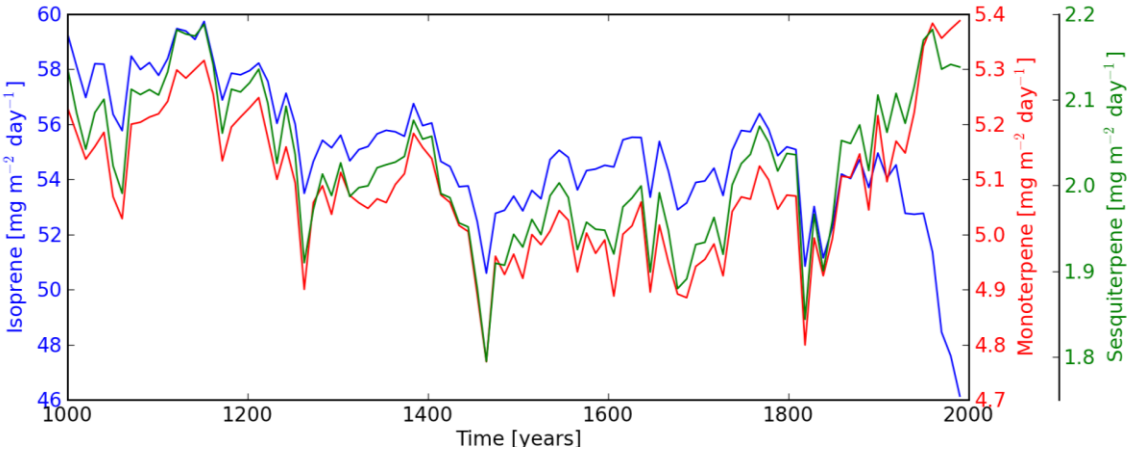

Figure 3.4. Globally averaged isoprene (blue), monoterpene (red) and sesquiterpene (green) emissions over the time period 1000-1990.

3.3 Methods

In this study we use a global chemical transport model with online aerosol microphysics to test the sensitivity of the simulated aerosol size distributions to anthropogenic changes in BVOC emissions from the years 1000 to 1990. Our goals are to determine the regional impact of anthropogenic BVOC emission changes on CCN number concentrations.

3.3.1 Model Description

In this study, we use the global chemical-transport model, GEOS-Chem (www.geos-chem.org), combined with the online aerosol microphysics module, TOMAS (GEOS-Chem-TOMAS) (as described in Pierce et al. (2013)) to test the sensitivity of global aerosol size distributions to changes in BVOC emissions. GEOS-Chem-TOMAS uses GEOS-Chem v9.01.02 with 4°x5° horizontal resolution, 47 vertical layers from the surface to 0.01 hPa with meteorological inputs from the GEOS5 reanalysis (http://gmao.gsfc.nasa.gov). TOMAS in this work simulates the aerosol size distribution using 15 size sections ranging from 3 nm to 10 μm. Nucleation rates in all simulations were predicted by ternary homogeneous nucleation of sulfuric acid, ammonia and water based on the parameterization of Napari et al. (2002) scaled down globally by a constant factor of 10^{-5} which has been shown to predict nucleation rates closer to measurements than other commonly used nucleation schemes (Jung et al., 2010; Westervelt et al., 2013). All emissions except terpenoid biogenic emissions (monoterpenes, isoprene and sesquiterpenes) in GEOS-Chem are described in van Donkelaar et al. (2008). The three dominant BVOC classes (monoterpenes, isoprene and sesquiterpenes) are included in GEOS-Chem using modeled reconstructions as provided by Acosta Navarro et al. (in prep) (this will be described in more detail in section 3.2.2). The emissions from Acosta Navarro et al. (in prep) override biogenic emissions previously input from the Model of Emissions and Gases and Aerosols from Nature (MEGAN) (Guenther et al., 2006) in the standard version of GEOS-Chem.

Traditionally, SOA in GEOS-Chem-TOMAS is formed only from terrestrial biogenic sources, with the biogenic source being a fixed yield of 10% of the monoterpene

emissions. However, isoprene and sesquiterpenes also serve as SOA precursors (Hoffmann et al., 1997; Griffin et al., 1999a; Kroll et al., 2006). In this study, we form SOA from monoterpenes, isoprene and sesquiterpenes with fixed yields of 10%, 3% and 20% respectively based on estimations summarized in Pye et al. (2010). The yields used in this study are on the low end of emission estimates; however, future work that we will do before submitting this manuscript to a peer-reviewed journal involves testing upper bounds on these yields (20%, 10% and 40%, respectively). In this study, particles are assumed to undergo kinetic, gas-phase-diffusion-limited growth with condensation of SOA proportional to the Fuchs-corrected aerosol surface area (Riipinen et al., 2011; D'Andrea et al., 2013). This kinetic condensation of SOA assumes low-volatility SOA with average saturation vapor pressure, C*, of less than approximately 10^{-3} μg m^{-3}. This assumption helped to yield the best agreement with present-day observed size distributions in D'Andrea et al. (2013) (chapter 2 of this thesis). Also as described in D'Andrea et al. (2013) (chapter 2 of this thesis), an additional 100 Tg yr^{-1} of SOA correlated with anthropogenic carbon monoxide emissions is required to match present-day measurements; however, in this study so far, the additional SOA is not included but will be included in the submitted manuscript.

We note that the predicted size distributions and uncertainty ranges in this paper are sensitive to the nucleation scheme, anthropogenic emissions fluxes and emissions size (e.g. Pierce et al. 2009c), but here we explore the modeled partial derivatives to changes in BVOC emissions only. Simulations for present-day anthropogenic emissions were run for 2005 meteorology with three months of spin-up from a pre-spun-up restart file. Simulations for pre-industrial anthropogenic emissions were run with anthropogenic emissions turned off. We test the sensitivity of predicted size distributions to anthropogenically driven changes in BVOC emissions in GEOS-Chem-TOMAS using four simulations (Table 3.1). First, we assume present-day anthropogenic emissions and have one simultaneous monthly mean BVOC emissions from the decadal average over the time periods years 1000-1010 (simulation BE1_AE2) and another simulation averaged over the years 1980-1990 (simulation BE2_AE2) (the justification of these time periods is explained in section 3.3.3). This method isolates the change in BVOCs and the

effect on aerosol size distributions under fixed anthropogenic emissions. We also test the sensitivity to changes in BVOC emissions over the same periods with no anthropogenic emissions to simulate a pre-industrial anthropogenic environment (simulations BE1_AEOFF and BE2_AEOFF). Using these four simulations, we also test the sensitivity of predicted size distributions to changes in anthropogenic emissions under present-day BVOC emissions by comparing simulations (simulation BE2_AEOFF and BE2_AE2). We repeat this test for year-1000 conditions by comparing BE1_AEOFF and BE1_AE2.

Table 3.1 Summary of GEOS-Chem-TOMAS simulations performed in this study.

Anthropogenic Emissions	Biogenic Emissions: 1000 – 1010	Biogenic Emissions: 1980 – 1990
2005	BE1_AE2	BE2_AE2
OFF	BE1_AEOFF	BE2_AEOFF

3.3.2 BVOC emissions

Modeled terpenoid BVOC emissions in this study are reconstructed for the years 1000 to 1990 by Acosta Navarro et al. (in prep) for the three dominant classes of BVOC (isoprene, monoterpenes and sesquiterpenes). This is described in detail by Acosta Navarro et al. (in prep), but will be summarized here. This modeled reconstruction was evaluated offline using numerical MEGAN (MEGAN v2.04 (Guenther et al., 2006)) over the time span of one millennium, with three-hour resolution and a spatial resolution of 3.75° x 3.75°. The version of MEGAN used in this inventory is a simplified version of Guenther et al., 2006, with 6 plant functional types instead of the standard 15 and smaller monoterpene light dependency factors (Acosta Navarro et al., in prep). Surface air temperature, downward solar radiation at the surface, soil water content (Jungclaus et al., 2010) and leaf area index (Pongratz et al., 2008, Pongratz et al., 2009) were simulated

using the Max-Planck Institute Earth System Model (MPI-ESM). Annual carbon dioxide (CO_2) concentrations were estimated using ice core samples from Law-Dome Antarctica (McFarling Meure et al., 2006). The vegetation maps were taken from the LPJ Dynamic Global Vegetation Model (LPJ-DGVM) (Kaplan et al., 2010, Pongratz et al., 2008) and soil wilting point fields were taken from MEGAN database (Guenther et al., 2006). Land-use cover was empirically developed by Kaplan et al., 2010 and estimates anthropogenic vegetation types such as crops and pastures. The model developed by Kaplan et al., 2010 estimates the percentage of land covered by 8 natural and 3 anthropogenic vegetation types. MEGAN was then run offline in a series of simulations testing sensitivities to the variables described above, and a millennium terpenoid BVOC emission inventory was created. Figure 3.5 shows the total mean millennial BVOC emissions (isoprene + monoterpenes + sesquiterpenes) in mg m^{-2} day^{-1} from the modeled reconstruction by Acosta Navarro et al. (in prep).

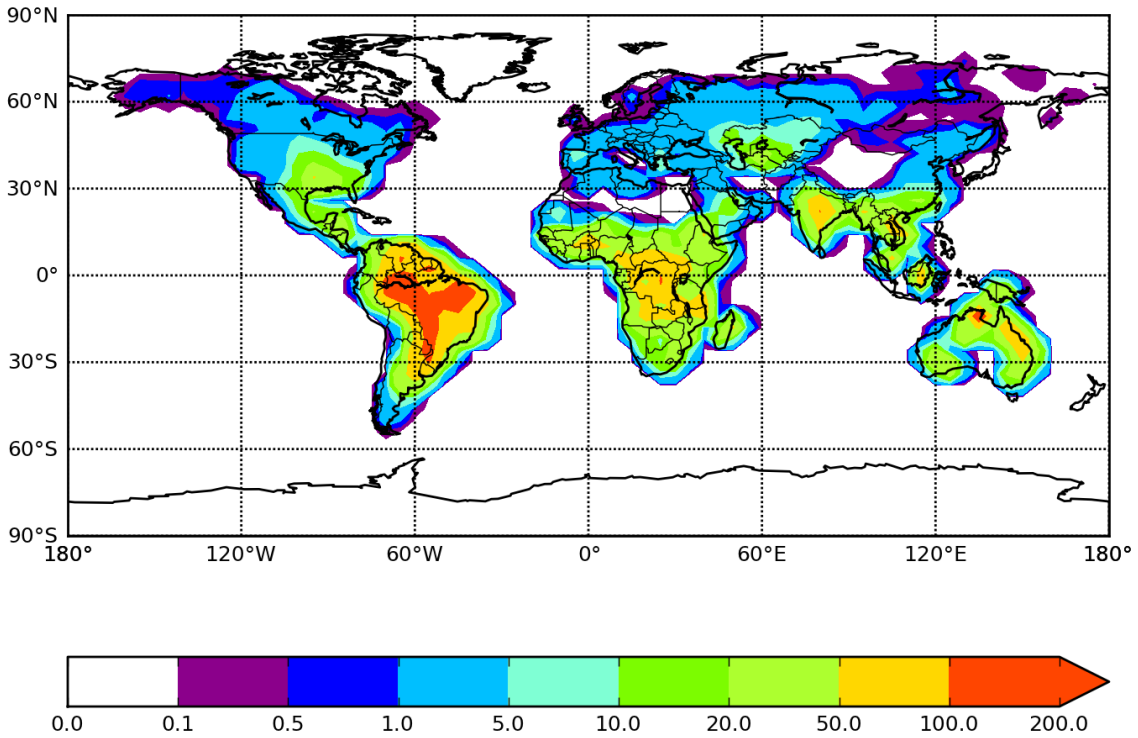

Figure 3.5. Total mean millennial BVOC emissions (isoprene + monoterpenes + sesquiterpenes) in mg m^{-2} day^{-1}.

The terpenoid BVOC emissions in Acosta Navarro et al. (in prep) are sensitive to variations in meteorological conditions and land-use changes, but are also sensitive to the empirical standard emission factors used in the developing of the inventory. Plant emission factors of the three BVOCs were averaged over wide plant families in order to make the model computationally feasible. Therefore, the changes in isoprene, monoterpenes and sesquiterpenes in the reconstruction are indicators of the response of the three BVOCs to external stresses and land-use change, rather than exact emission estimates. Also, changing the resolution of the emissions inventory from the original resolution to a coarser resolution may inherently have uncertainties.

3.4 Results

3.4.1 Changes to SOA formation rates

Figure 3.6a shows the mean millennial fixed yield SOA formation from BVOC emissions (monoterpenes, isoprene and sesquiterpenes) in mg m^{-2} day^{-1} over the years 1000-1990. The spatial distribution of SOA formation is collocated with total millennial BVOC emissions as seen in Figure 3.5. Figure 3.6c shows the percent change in fixed-yield SOA formation from the same averaged BVOC emissions (monoterpenes, isoprene and sesquiterpenes) between the periods 1000-1010 and 1980-1990 ("present day" – "pre-industrial"). An increase in SOA formation is represented by red colors, and a decrease in SOA formation by blue. This figure shows the spatial variation in changes in SOA formation over the last millennium due to historical changes in monoterpene, isoprene and sesquiterpene emissions. Regions such as central North America, eastern Australia, and southern South America show significant decreases, exceeding 75% in SOA formation. There are also regions such as India, and southeast Asia with increases of greater than 50% in SOA formation. These changes in emissions are solely due to millennial anthropogenic influences on BVOC emissions. Figure 3.6b shows the absolute change in fixed-yield SOA formation from averaged BVOC emissions (monoterpenes, isoprene and sesquiterpenes) between the periods 1000-1800 and 1950-1990 ("present day" – "pre-industrial") in mg m^{-2} day^{-1}. In Figure 3.6c, there are regions

with large percent increases or decreases in SOA formation, such as the Sahara, central Australia, and central Eurasia; however, the absolute change is negligible in these regions due to very low emissions (as seen in Figure 3.5). Meaningful decreases/increases in SOA formation would significantly decrease/increase the amount of low-volatility condensable organic material available to grow nanoparticles in the atmosphere. Therefore, changes in SOA formation of this magnitude could have an important anthropogenic aerosol effect on regional climates.

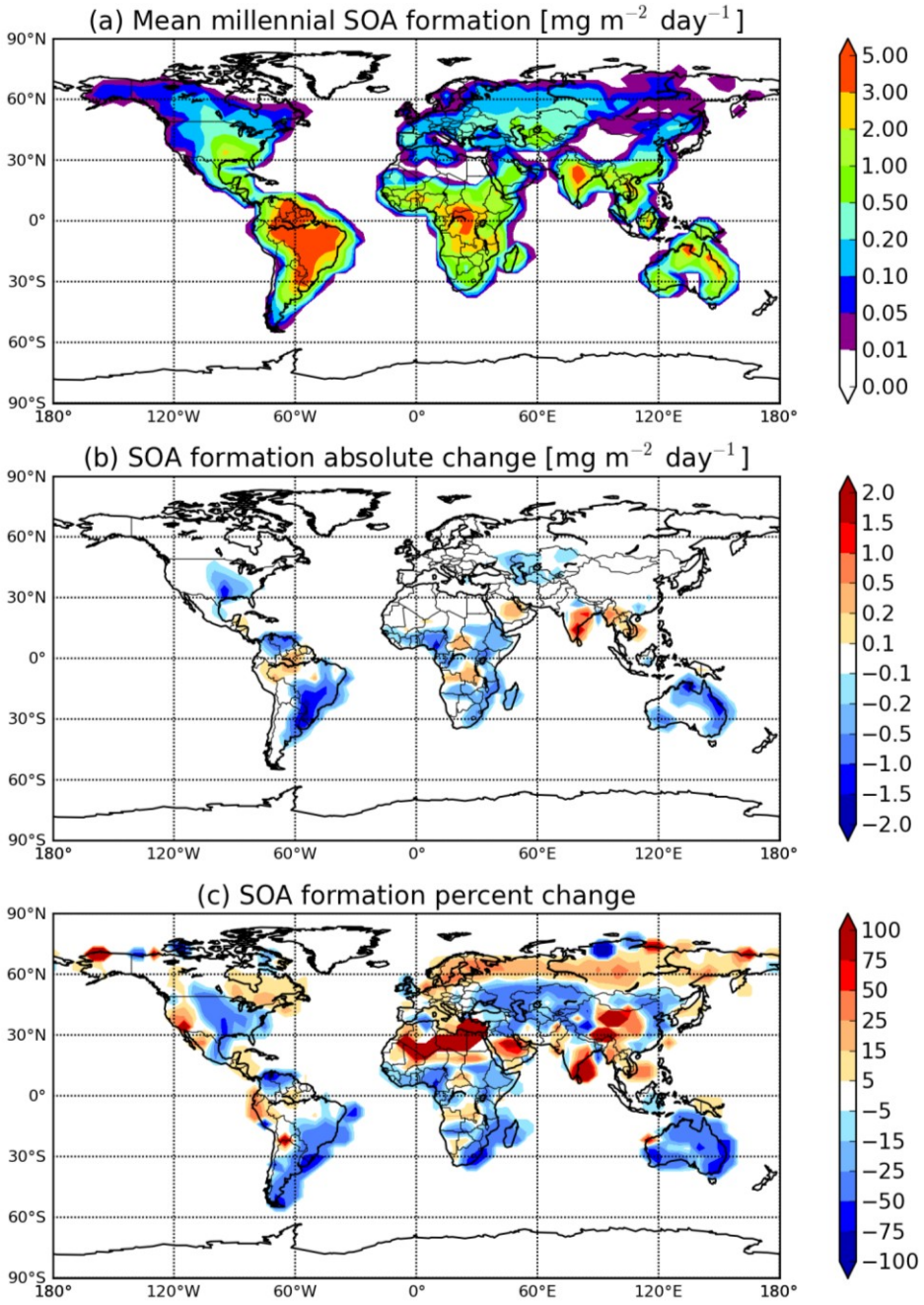

Figure 3.6. (a) Mean millennial fixed yield SOA formation between the periods 1000-1990 in mg m^{-2} day^{-1}, (b) absolute change in fixed yield SOA formation from averaged BVOC emissions (monoterpenes, isoprene and sesquiterpenes) between the periods 1000-1010 and 1980-1990 ("present day" – "pre-industrial") in mg m^{-2} day^{-1}, and (c) Percent change in fixed yield SOA formation from averaged BVOC emissions (monoterpenes, isoprene and sesquiterpenes) between the periods 1000-1010 and 1980-1990 ("present day" – "pre-industrial"). An increase in SOA formation in (b) and (c) is represented by red colors, and a decrease in SOA formation by blue.

Changes over the past millennium in all three classes of terpenoid BVOCs (Figure 3.4) combine to impact SOA formation in the atmosphere. Figure 3.7 shows the percent contribution to SOA formation by (a) isoprene, (b) monoterpene and (c) sesquiterpene emissions, averaged over the years 1000-1990. The area enclosed by the red contour represents greater than 5% of the maximum mean millennial emissions of all BVOCs (isoprene + monoterpenes + sesquiterpenes) in mg m^{-2} day^{-1} (7.7 mg m^{-2} day^{-1}) (see Figure 3.5 for total mean millennial BVOC emissions). Isoprene (Figure 3.7a) has the largest contribution to SOA formation with a global millennial mean contribution of 64%. Regions where isoprene emissions have significant contributions to SOA formation (greater than 70%) are collocated with regions of highest total BVOC emissions (red contour). This shows that significant changes in isoprene emissions over the past millennium in these regions are the predominant cause of changes in SOA formation. Monoterpene emissions (Figure 3.7b) contribute to 20% of global mean millennial SOA formation. Figure 3.7b indicates that changes in monoterpene emissions are the most important cause of SOA formation in the northern hemisphere boreal-forested regions, with contributions exceeding 80%. However, monoterpenes contribute less than 20% in regions with the highest total emissions. Sesquiterpene emissions represent the smallest global mean contribution to SOA formation at 16% over the past millennium. Unlike isoprene and monoterpene emissions that have clear regional importance, Figure 3.7c indicates that sesquiterpene emissions tend to have a more uniform contribution to SOA formation across all vegetated regions, rarely exceeding 20%.

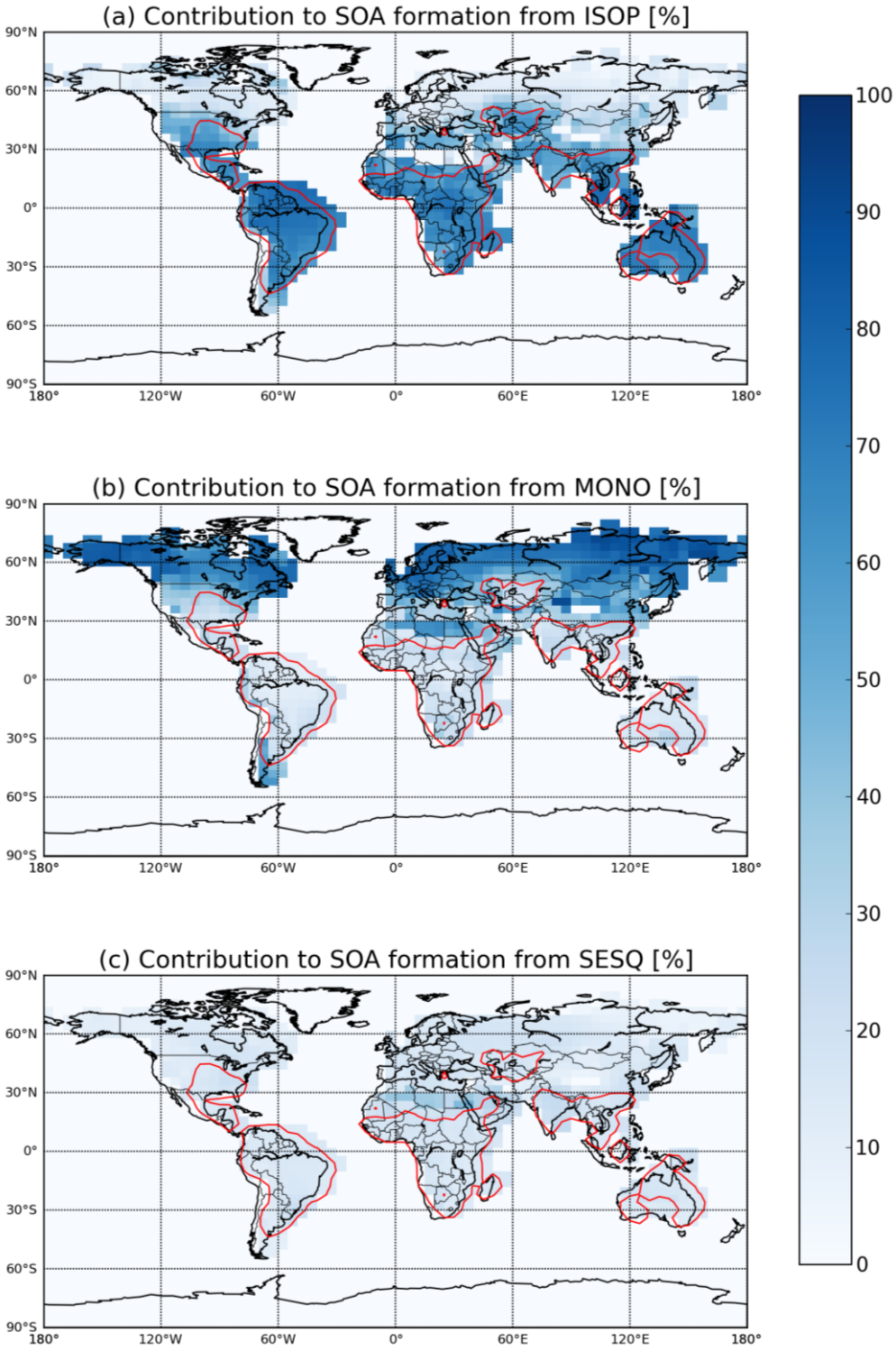

Figure 3.7. Percent contribution to SOA formation by (a) isoprene, (b) monoterpene and (c) sesquiterpene emissions, averaged over the years 1000-1990. The area enclosed by the red contour represents greater than 5% of the maximum mean millennial emissions of BVOCs (isoprene + monoterpenes + sesquiterpenes) in mg m^{-2} day^{-1} (7.7 mg m^{-2} day^{-1}).

3.4.2 Impact on CCN number: changing BVOC emissions

Figure 3.8 shows the change in (a) N3, (b) N10, (c) N40 and (d) N80 (number of particles with diameter greater than 3 nm, 10 nm, 40 nm and 80 nm respectively) when changing BVOC emissions from pre-industrial (average emissions from 1000-1010) to present-day (average emissions from 1980-1990) with constant present day anthropogenic emissions (2005) (BE2_AE2 – BE1_AE2). Comparing these two simulations isolates the effect of millennial changes in BVOC emissions on particle size distributions. Globally averaged, N3 and N10 increased by 1.9% and 1.5% respectively, whereas N40 and N80 decreased by 0.5% and 1.4% respectively. There are decreases in N80 (our proxy for CCN sized particles) exceeding 50% in regions such as southern South America, southern Africa, southeastern North America and Australia. These regions coincide with regions of significant decrease in isoprene emissions (Figure 3.1) and SOA formation (Figure 3.6). The relationship between the decrease in isoprene emissions and SOA formation with the decrease in N80 can be explained through microphysical feedback mechanisms. Firstly, the decrease in total isoprene emissions in these regions causes a decrease in SOA formation as explained in section 3.4.1. With decreases in SOA formation, ultrafine particle growth decreases due to the reduction in available condensable material. This can be seen in Figure 3.8a and 3.8b where increases in N3 and N10 are collocated. This suppression of ultrafine particle growth limits the number of particles that can grow to CCN sizes, hence decreasing N80 in these regions. This can be seen in Figure 3.8c and 3.8d, where regions of increasing N3 and N10 coincide with regions of decreasing N40 and N80. Throughout these regions, N3 and N10 increases exceed 50%, and decreases in N40 and N80 exceed 50%. These are significant changes in CCN concentrations in these regions due largely to changes in BVOCs due to anthropogenic land-use changes. With significant decreases in N40 and N80, the condensation sink for sulfuric acid (H_2SO_4) and coagulation sink for ultrafine particles would also decrease. This would increase the survival probability of ultrafine particles and hence increase N3 and N10. Thirdly, with a decrease in SOA formation and a decrease in ultrafine particle growth, the concentration of sulfuric acid (H_2SO_4) vapor would increase in these regions due to a decrease in the

condensation sink. This would increase nucleation due to the strong dependence on H_2SO_4 vapor concentrations. Therefore, increased nucleation increases the number of freshly nucleated particles and N3.

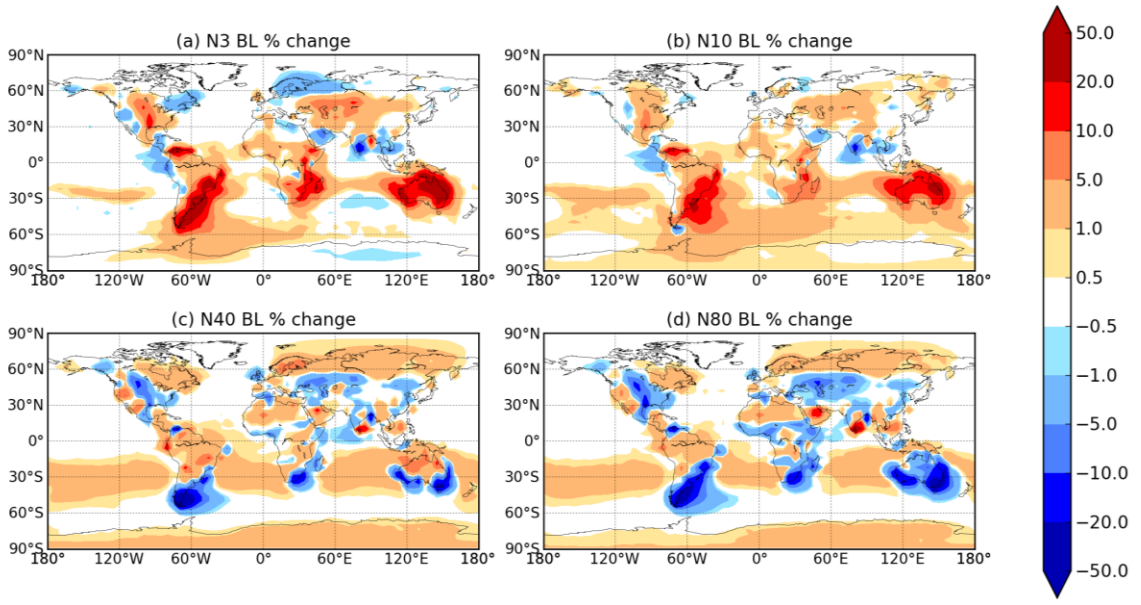

Figure 3.8. Change in (a) N3, (b) N10, (c) N40 and (d) N80 (number of particles with diameter greater than 3 nm, 10 nm, 40 nm and 80 nm respectively) when changing BVOC emissions from pre-industrial (average emissions from 1000-1010) to present-day (average emissions from 1980-1990) with constant present day anthropogenic emissions (2005) (BE2_AE2 – BE1_AE2). Globally averaged, N3 and N10 increased by 1.9% and 1.5% respectively, whereas N40 and N80 decreased by 0.5% and 1.4% respectively.

Figure 3.9 shows the change in (a) N3, (b) N10, (c) N40 and (d) N80 when changing BVOC emissions from pre-industrial (average emissions from 1000-1010) to present-day (average emissions from 1980-1990) with anthropogenic emissions turned off (BE2_AEOFF – BE1_AEOFF). Globally averaged, N3, N10 and N40 increased by 2.8%, 2.4% and 1.0% respectively, whereas N80 decreased by 0.4%. Similar to the previous case, globally averaged N3 and N10 increased over the past millennium. However, contrary to the previous case, with anthropogenic emissions turned off, globally averaged N40 also increased. The spatial patterns in globally averaged number of CCN sized particles (N80) in this simulation reflected the same decreasing trend as

Figure 3.8. In Figure 3.9, the regions of increasing N3 and N10 coincide with regions of decreasing N40 and N80, following the same spatial pattern as Figure 3.8.

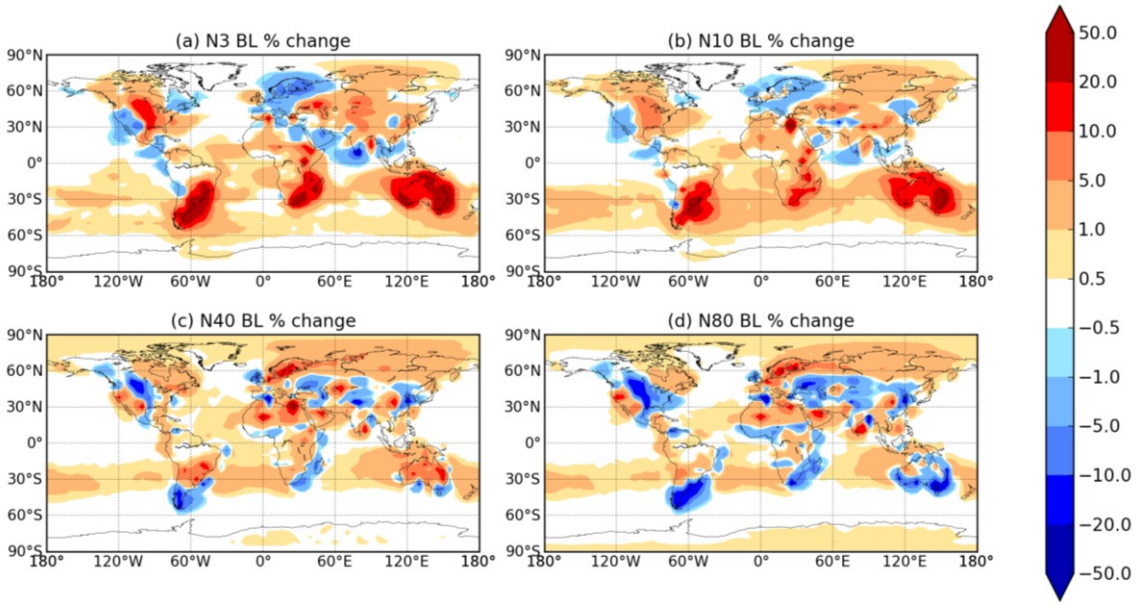

Figure 3.9. Change in (a) N3, (b) N10, (c) N40 and (d) N80 (number of particles with diameter greater than 3 nm, 10 nm, 40 nm and 80 nm respectively) when changing BVOC emissions from pre-industrial (average emissions from 1000-1010) to present-day (average emissions from 1980-1990) with anthropogenic emissions turned off (BE2_AEOFF – BE1_AEOFF). Globally averaged, N3, N10 and N40 increased by 2.8%, 2.4% and 1.0% respectively, whereas N80 decreased by 0.4%.

The microphysical feedback mechanisms in this comparison (BE2_AEOFF – BE1_AEOFF) are the same as the previous comparison (BE2_AE2 – BE1_AE2); however, the magnitude of the millennial changes in particle number concentrations differs. With anthropogenic emissions turned off to simulate pre-industrial conditions, changes in number concentrations of particles in all size ranges are shifted towards more positive changes than the simulation with present day anthropogenic emissions. This is caused by the difference in total particle number concentrations and the mean size of the particles. As seen in Figure 3.10, present-day anthropogenic conditions have more than 4x more particles by number than in pre-industrial conditions and the mean diameter is at smaller sizes. The mean diameter in the simulation with present-day anthropogenic

conditions is 27.1 nm, whereas the simulation with pre-industrial anthropogenic conditions had a mean diameter of 41.1 nm. Therefore, there are an increased number of ultrafine particles competing for condensation of SOA and growth to CCN sizes in the simulations with anthropogenic emissions on, and the particles in these simulations are (on average) smaller and further from CCN sizes. Thus, ultrafine particles grow to CCN sizes more efficiently to 40 and 80 nm in the simulations with anthropogenic emissions turned off and are more susceptible to BVOC changes because there are fewer particles competing for condensable material and the mean size is larger. The fractional changes in N3 are larger in the cases with anthropogenic emissions off because there are fewer particles overall. Thus, there is a smaller increase in N3 and larger decrease in N80 than with anthropogenic emissions turned off.

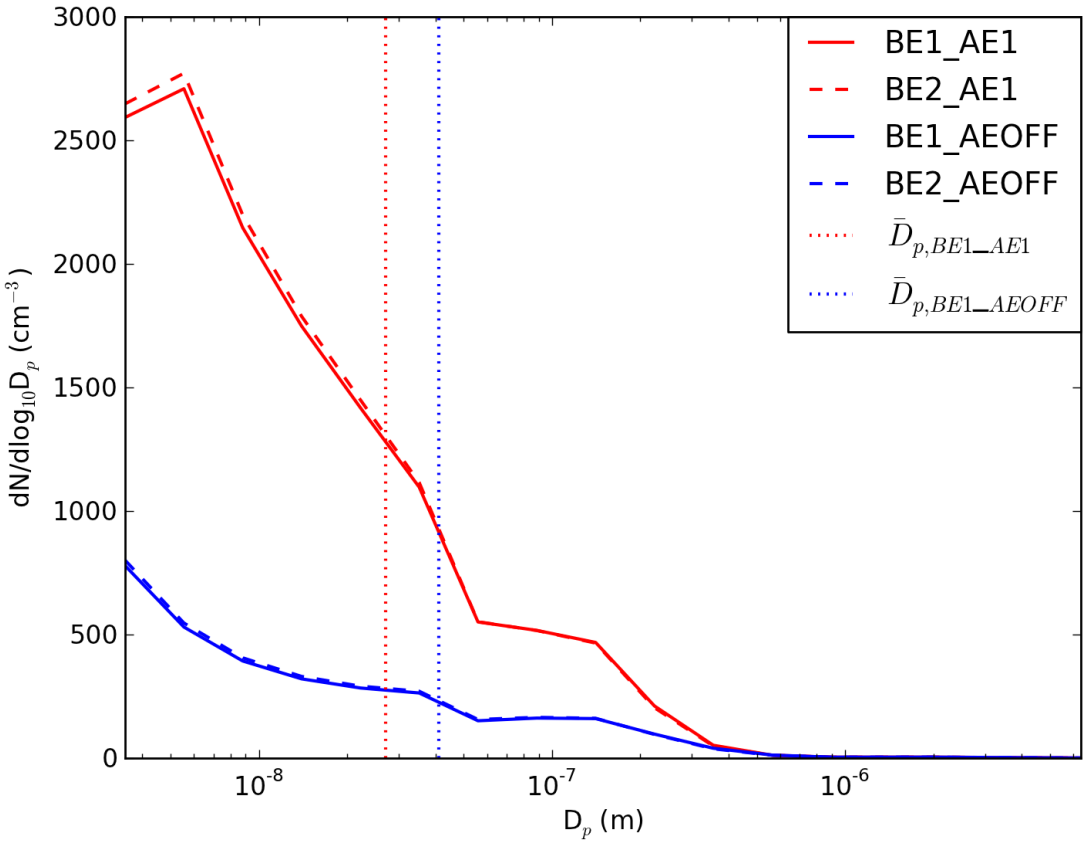

Figure 3.10. Simulated global annual-mean particle number size distributions for the simulations outlined in Table 3.1. The red and blue vertical dotted lines represent the mean diameter for the simulations including anthropogenic emissions (BE1_AE1) and without anthropogenic emissions (BE1_AEOFF) respectively.

The effect on particle numbers by changing anthropogenic emissions under fixed BVOC emissions was also investigated. The globally averaged change in N3, N10, N40 and N80 when changing anthropogenic emissions from pre-industrial (off) to present-day (2005) with constant present-day BVOC emissions (average biogenic emissions from 1980-1990) (BE2_AE2 – BE2_AEOFF) increased by 346%, 350%, 218% and 168% respectively. These sensitivities to anthropogenic emissions changed only modestly when biogenic emissions from 1000-1010 were used (BE1_AE2 – BE1_AEOFF): globally averaged N3, N10, N40 and N80 all increased by 350%, 354%, 223% and 171% respectively. Thus, the historic state of BVOC emissions have little effect on the impact of anthropogenic size distributions on aerosol concentrations; therefore, we have not included figures and a more-detailed comparison.

3.5 Conclusions

In this study, we investigated the impact of millennial changes in biological volatile organic compound (BVOC) emissions on secondary organic aerosol (SOA) formation and global aerosol size distributions. We used the global aerosol microphysics model GEOS-Chem-TOMAS to connect the historical changes in BVOC emissions to particle size distributions and the number concentration of cloud condensation nuclei (CCN).

This study built off recent work by Acosta Navarro et al. (in prep) who determined how BVOC emissions have changed in the past millennium due to changes in land use, temperature, and carbon dioxide (CO_2) concentrations. They used a model reconstruction of the three dominant classes of BVOC emissions (isoprene, monoterpenes and sesquiterpenes) to simulate decadal-averaged monthly mean emissions over the time period 1000-1990. Their emissions reconstruction predicted that isoprene emissions decreased over the past millennium (due mainly to anthropogenic land-use changes), whereas monoterpene and sesquiterpene emissions increased (due predominantly to temperature increases). In our work, we included these millennial emissions into the GEOS-Chem-TOMAS chemical-transport model with online aerosol microphysics. We

assumed that isoprene, monoterpenes and sesquiterpenes form SOA in GEOS-Chem-TOMAS via fixed yields of 3%, 10% and 20% respectively.

When anthropogenic emissions (eg. SO_2, NO_x, primary aerosols) were held at present day values and emissions of isoprene, monoterpenes and sesquiterpenes changed from year 1000-1010 values ("pre-industrial") to year 1980-1990 values ("present day"), N80 (the number of particles with diameter greater than 80 nm, our proxy for CCN in this study) had decreases of greater than 50% in years 1980-1990 relative to years 1000-1010 that were predicted in regions with extensive land-use changes such as southern South America, southern Africa, southeastern North America and Australia since year 1000. This significant change in N80 was predominantly driven by anthropogenic changes in high BVOC-emitting vegetation to lower emitting crops/grazing land. Similar sensitivities in N80 exist when BVOC emissions were changed over the same time period but with anthropogenic emissions turned off.

When BVOC emissions were held at present day values, and anthropogenic emissions changed from turned off ("pre-industrial") to 2005 ("present day") values, there were globally averaged increases in number concentrations of all particle sizes. N80 increased by 168% in present day relative to pre-industrial due to large increases in particle emissions from industrial development. Similar sensitivities exist when anthropogenic emissions were changed over the same time period but with BVOC emissions at pre-industrial values. Thus, the change in BVOCs should have little impact on the radiative forcing of anthropogenic pollution.

There are inherent uncertainties in the millennial BVOC emission reconstruction from Acosta Navarro et al. (in prep) used in this study. Averaged emission factors were used over wide plant families and thus the millennial changes in isoprene, monoterpenes and sesquiterpenes are indicators of the response of the three BVOCs to anthropogenic influences as opposed to exact estimations of the emissions. Before submission of the paper, we will also include simulations using a different set of historical emissions from the dynamic vegetation model LPJ-GUESS (Sitch et al., 2003; Smith et al., 2001; Bondeau et al., 2007). We will also include simulations testing the sensitivity of particle size distributions to different yields of SOA.

While present-day emissions of anthropogenic aerosols are a significant contributor to climate change, this study has shown the importance of anthropogenically driven changes in BVOC emissions over the past millennium on SOA formation and CCN number concentrations. The large decrease in CCN due to land-use changes over the past millennium appears to be a largely overlooked and important anthropogenic aerosol effect on regional climates.

CHAPTER 4 CONCLUSIONS

4.1 Summary

Global climate change is one of the most important issues currently impacting human activity. However, quantifying the impact of humans on global climate change is very uncertain. One of the most uncertain factors according to the Intergovernmental Panel on Climate Change Fourth Assessment Report is the effect of anthropogenic aerosols on the radiative forcing on the Earth's climate (IPCC, 2007). Aerosols scatter and absorb incoming solar radiation, directly affecting Earth's climate. Aerosols also modify cloud properties, altering the amount of solar radiation reflected by clouds, which indirectly affects Earth's climate. To quantify the direct and indirect effect of aerosols, the primary tools used for predicting global climate change are global aerosol models that involve online aerosol microphysics in global climate models (GCMs) or chemical transport models (CTMs). The accuracy of modeled predictions of clouds and climates however, are highly dependent upon correctly simulating aerosol size and number. The influence of aerosols on clouds and ultimately climate is driven by the number concentration of cloud condensation nuclei (CCN), or aerosols with diameters larger than about 50 nm (Pierce et al., 2007). Thus, CCN concentrations are highly dependent on the number, size and composition of particles. Many physical and chemical processes shape the number, size and composition of particles including emissions, nucleation, condensation of vapors and deposition. Each of these processes has uncertainties and is imperfectly represented in global aerosol simulations (Lee et al., 2013). Therefore, in order to accurately quantify the aerosol impact on climate change, the size distribution and ultimately growth of atmospheric aerosols must be properly represented in GCMs. In this thesis, we specifically looked at condensable secondary organic vapors and their effects on the aerosol size distribution and CCN.

This thesis involved two individual projects. The first project involved using a global chemical transport model with online aerosol microphysics to simulate the effect

of chemically produced organic aerosol (secondary organic aerosol, SOA) on particle size distributions in the atmosphere. The model simulations were compared to various global measurement sites in an effort to constrain the model. We found that the amount and volatility of SOA has a drastic impact on the number concentration of climatically relevant particles. We found that, in order to match global measurements, a large amount (100 Tg yr^{-1}) of SOA correlated with anthropogenic carbon monoxide emissions had to be included into the model, and a significant fraction of the SOA had to condense as nonvolatile. We also investigated the impact of two sub-20 nm size-dependent growth rate parameterizations on simulated particle size distributions (Häkkinen et al., 2013; Kuang et al., 2012). We found that these parameterizations have little impact on global climatically relevant particle number concentrations; however, they may have a significant regional impact. This research improves the predictions of climatically relevant particles in global climate simulations.

The second project investigates the effect of changing biogenic volatile organic compound (BVOC) emissions (from changing land use, temperature and CO_2) on climatically relevant particles through SOA formation. We incorporated recent estimates of present-day and pre-industrial biogenic volatile organic emissions (specifically isoprene, monoterpenes and sesquiterpenes) into a global chemical transport model with online aerosol microphysics. We have found that millennial changes in isoprene emissions are the primary driver of SOA formation. Decreases in isoprene emissions exceeding 75% due to land-use changes in regions such as central North America, eastern Australia, and southern South America, cause decreases exceeding 75% in SOA formation. This decrease in SOA formation has large implications on climatically relevant particles, causing decreases in excess of 50% in CCN sized particles. This change in CCN may be a largely overlooked and important anthropogenic aerosol effect on regional climates

4.2 Future Work

The first study in this thesis (chapter 2) has shown the importance of correctly simulating the amount and condensational behavior of SOA in global aerosol microphysics models. The inclusion of an extra 100 Tg yr^{-1} of SOA correlated with anthropogenic carbon monoxide (CO) drastically improved the accuracy of particle size distributions in the model when compared to global measurement sites. The chemistry involved with the additional source of low-volatility SOA is most likely due to pollution-driven anthropogenic enhancement of SOA formation from BVOCs. Once the chemical mechanisms of this enhanced SOA formation have been determined, future work would involve investigating the chemistry involved in the formation of this additional SOA source as well as incorporating a more mechanistic approach to SOA formation in the model rather than solely correlating with anthropogenic CO emissions. Also in the first study, assuming low volatile SOA, or condensation proportional to the Fuchs-corrected aerosol surface-area, increased the accuracy of the model when compared with measurements. Improved representations of the chemical and physical processes forming low-volatility SOA in the model, such as gas-phase oxidation or particle-phase acid-base reactions and polymerization reactions, could be investigated and included in the model. Also, the model output from this study could be incorporated into a radiative transfer model to quantitatively determine the radiative forcing effect on climate due to the additional low-volatility SOA.

The second study (chapter 3) in this thesis found that anthropogenic changes in biogenic emissions over the past millennium have had a significant impact on CCN number concentrations in the atmosphere. These changes in CCN may be a largely overlooked anthropogenic aerosol effect and have future climatic implications. This work has not yet been submitted to a peer-reviewed journal, and I will perform and include several more tests and analyses before submission. Future work involves incorporating the assumptions investigated in chapter 2 into this study. The simulations in this study assume low volatile SOA with condensation proportional to the aerosol surface area, but the additional 100 Tg yr^{-1} of SOA correlated with anthropogenic carbon

monoxide emissions has not been included yet. The additional SOA will be added in simulations to investigate the influence this extra SOA will have with millennial changes in biogenic emissions. Also, future work for this project involves incorporating another set of millennial emissions derived from a different model (LPJ-GUESS) to test the robustness of this anthropogenic aerosol effect rather than just relying on one model prediction of these emissions. The simulations used in this study were also performed with biogenic emissions for the years 1000-1010 and 1980-1990 only. The emissions of isoprene, monoterpenes and sesquiterpenes around 1800 appear to reach a local minimum. The anthropogenic influence on the BVOC emissions (decreases in all three terpenoids due to deforestation) occurs throughout the period from years 1000 to 1800, before monoterpenes and sesquiterpenes begin to increase (due to increased carbon dioxide concentrations and temperature increases) after 1800. Therefore, it would be beneficial to compare model runs for a time period around 1800 to help understand the effects of land-use change, as well as carbon dioxide and temperature increases, on SOA formation and CCN number concentrations over the past millennium. Future work would involve running simulations for different time periods over the past millennium, more specifically around the year 1800 (see Figure 3.4). Also, similar to the previous study, including this model output in a radiative transfer model would help to quantify this anthropogenic aerosol effect on climate. Finally, I will test the sensitivity of our results to different assumed SOA yields.

BIBLIOGRAPHY

1) Aalto, P.P., K. Hämeri, E. Becker, R. Weber, J. Salm, J.M. Mäkelä, C. Hoell, C.D. O'Dowd, H. Karlsson, H-C. Hansson, M. Väkevä, I. Koponen, G. Buzorius, and M. Kulmala, Physical characteristics of aerosol particles during nucleation events. in press Tellus B, 53, 344-345,, 2001.
2) Adams, J. M., Constable, J. V., Guenther, A. B., & Zimmerman, P.: An estimate of natural volatile organic compound emissions from vegetation since the last glacial maximum, Chemosphere-Global Change Science, 3, 73-91, 2001.
3) Adams, P. J. and Seinfeld, J. H.: Predicting global aerosol size distributions in general circulation models, Journal of Geophysical Research-Atmospheres, 107(D19), 4310–4370, 2002.
4) Adams, P. J. and Seinfeld, J. H.: Disproportionate impact of particulate emissions on global cloud condensation nuclei concentrations, Geophys. Res. Lett., 30, 1210–1239, doi:10.1029/2002GL016303, 2003.
5) Albrecht, B. A.: Aerosols, Cloud Microphysics, and Fractional Cloudiness, Science, 245, 1227-1230, 1989.
6) Arneth, A., Monson, R. K., Schurgers, G., Niinemets, Ü., & Palmer, P. I.: Why are estimates of global terrestrial isoprene emissions so similar (and why is this not so for monoterpenes)?, Atmospheric Chemistry and Physics, 8, 4605-4620, 2008.
7) Asmi, A., Wiedensohler, A., Laj, P., Fjaeraa, A.-M., Sellegri, K., Birmili, W., Weingartner, E., Baltensperger, U., Zdimal, V., Zikova, N., Putaud, J.-P., Marinoni, A., Tunved, P., Hansson, H.- C., Fiebig, M., Kiveks, N., Lihavainen, H., Asmi, E., Ulevicius, V., Aalto, P. P., Swietlicki, E., Kristensson, A., Mihalopoulos, N., Kalivitis, N., Kalapov, I., Kiss, G., de Leeuw, G., Henzing, B., Harrison, R. M., Beddows, D., O'Dowd, C., Jennings, S. G., Flentje, H., Weinhold, K., Meinhardt, F., Ries, L., and Kulmala, M.: Number size distributions and seasonality of submicron particles in Europe 2008–2009, Atmos. Chem. Phys., 11, 5505–5538, doi:10.5194/acp-11-5505-2011, 2011.

8) Bondeau, A., Smith, P. C., Zaehle, S., Schaphoff, S., Lucht, W., Cramer, W., Gerten, D., Lotze-Campen, H., Müller, C., Reichstein, M., Smith, B.: Modelling the role of agriculture for the 20th century global terrestrial carbon balance. Global Change Biology, 13(3), 679-706, 2007.

9) Carlton, A. G., Pinder, R. W., Bhave, P. V., and Pouliot, G. A.: To What Extent Can Biogenic SOA be Controlled?, Environ. Sci. Technol., 44, 3376–3380, doi:10.1021/es903506b, 2010.

10) Carslaw, K. S., Boucher, O., Spracklen, D. V., Mann, G. W., Rae, J. G. L., Woodward, S., and Kulmala, M.: A review of natural aerosol interactions and feedbacks within the Earth system, Atmospheric Chemistry and Physics, 10, 1701-1737, 2010.

11) Charlson, R. J., Schwartz, S. E., Hales, J. M., Cess, R. D., Coakley, J. A., Hansen, J. E., and Hofmann, D. J.: Climate forcing by anthropogenic aerosols, Science, 255, 423–430, 1992.

12) Clement, A. C., Burgman, R., and Norris, J. R.: Observational and Model Evidence for Positive Low-Level Cloud Feedback, Science, 325, 460–464, 2009.

13) Croft, B., Pierce, J. R., Martin, R. V., Hoose, C., and Lohmann, U.: Uncertainty associated with convective wet removal of entrained aerosols in a global climate model, Atmos. Chem. Phys., 12, 10725-10748, doi:10.5194/acp-12-10725-2012, 2012.

14) deGouw, J. A., Middlebrook, A. M., Warneke, C., Goldan, P. D., Kuster, W. C., Roberts, J. M., Fehsenfeld, F. C., Worsnop, D. R., Canagaratna, M. R., Pszenny, A. A. P., Keene, W. C., Marchewka, M., Bertman, S. B., and Bates, T. S.: Budget of organic carbon in a polluted atmosphere: Results from the New England Air Quality Study in 2002, J. Geophys. Res., 110, D16305, doi:10.1029/2004JD005623, 2005.

15) D'Andrea, S. D., Häkkinen, S. A. K., Westervelt, D. M., Kuang, C., Levin, E. J. T., Kanawade, V. P., Leaitch, W. R., Spracklen, D. V., Riipinen, I., and Pierce, J. R.: Understanding and constraining global secondary organic aerosol amount and size-resolved condensational behavior, Atmos. Chem. Phys. Discuss., 13, 18969-19007, doi:10.5194/acpd-13-18969-2013, 2013.

16) Donahue, N. M., Robinson, A. L., and Pandis, S. N.: Atmospheric organic particulate matter: From smoke to secondary organic aerosol, Atmos. Environ., 43, 94–106, 2009.

17) Donahue, N. M., Trump, E. R., Pierce, J. R. and Riipinen, I.: Theoretical constraints on pure vapor-pressure driven condensation of organics to ultrafine particles, Geophysical Research Letters, 38(16), L16801, doi:10.1029/2011GL048115, 2011.

18) Dusek, U., Frank, G.P., Hildebrandt, L., Curtius, J., Schneider, J., Walter, S., Chand, D., Drewnick, F., Hings, S., Jung, D., Borrmann, S., Andreae, M.O.: Size Matters More Than Chemistry for Cloud-Nucleating Ability of Aerosol Particles, Science 312, 1375-1378, 2006.

19) Erupe, M. E., Benson, D. R., Li, J., Young, L.-H., Verheggen, B., Al-Refai, M., Tahboub, O., Cunningham, V., Frimpong, F., Viggiano, A. A., and Lee, S.-H.: Correlation of Aerosol Nucleation Rate with Sulfuric Acid and Ammonia in Kent Ohio: An Atmospheric Observation, J. Geophys. Res., 115, D23216, doi:10.1029/2005GL023268, 2010.

20) Fehsenfeld, F., Calvert, J., Fall, R., Goldan, P., Guenther, A. B., Hewitt, C. N., and Zimmerman, P.: Emissions of volatile organic compounds from vegetation and the implications for atmospheric chemistry, Global Biogeochemical Cycles, 6, 389-430, 1992.

21) Forster, P., Ramaswamy, V., Artaxo, P., Berntsen, T., Betts, R., Fahey, D. W., Haywood, J., Lean, J., Lowe, D. C., Myhre, G., Nganga, J., Prinn, R., Raga, G., Schulz, M., and Dorland, R. V.: Changes in Atmospheric Constituents and in Radiative Forcing, in: Climate Change 2007: The Physical Science Basis, Contribution of Working Group I to the Fourth Assessment Report of the Intergovernmental Panel on Climate Change, edited by: Miller, H. L., Cambridge University Press, Cambridge, UK and New York, NY, USA, 129-234, 2007.

22) Goldstein, A. H. and Gallbaly, I. E.: Known and unexplored organic constituents in the Earth's Atmosphere, Environ Sci. Technol., 41(5), 1514–1521, 2007.

23) Griffin, R. J., Cocker, D. R., Flagan, R. C., and Seinfeld, J. H.: Organic aerosol formation from the oxidation of biogenic hydrocarbons, J. Geophys. Res., 104, 3555–3567, 1999a.

24) Häkkinen, S. A. K., Manninen, H. E., Yli-Juuti, T., Merikanto, J., Kajos, M. K., Nieminen, T., D'Andrea, S. D., Asmi, A., Pierce, J. R., Kulmala, M., and Riipinen, I.: Semi-empirical parameterization of size-dependent atmospheric nanoparticle growth in continental environments, Atmos. Chem. Phys., 13, 7665-7682, doi:10.5194/acp-13-7665-2013, 2013.

25) Hallquist, M., Wenger, J. C., Baltensperger, U., Rudich, Y., Simpson, D., Claeys, M., Dommen, J., Donahue, N. M., George, C., Goldstein, A. H., Hamilton, J. F., Herrmann, H., Hoffmann, T., Iinuma, Y., Jang, M., Jenkin, M. E., Jimenez, J. L., Kiendler-Scharr, A., Maenhaut, W., McFiggans, G., Mentel, Th. F., Monod, A., Pr´evˆot, A. S. H., Seinfeld, J. H., Surratt, J. D., Szmigielski, R., and Wildt, J.: The formation, properties and impact of secondary organic aerosol: current and emerging issues, Atmos. Chem. Phys., 9, 5155–5236, doi:10.5194/acp-9-5155-2009, 2009.

26) Heald, C. L., Jacob, D. J., Park, R. J., Russell, L. M., Huebert, B. J., Seinfeld, J. H., Liao, H., and Weber, R. J.: A large organic aerosol source in the free troposphere missing from current models, Geophysical Research Letters, 32, no. 18: L18809, 2005.

27) Heald, C. L., Coe, H., Jimenez, J. L., Weber, R. J., Bahreini, R., Middlebrook, A. M., Russell, L. M., Jolleys, M., Fu, T.-M., Allan, J. D., Bower, K. N., Capes, G., Crosier, J., Morgan, W. T., Robinson, N. H., Williams, P. I., Cubison, M. J., DeCarlo, P. F., and Dunlea, E. J.: Exploring the vertical profile of atmospheric organic aerosol: comparing 17 aircraft field campaigns with a global model, Atmos. Chem. Phys., 11, 12673-12696, doi:10.5194/acp-11-12673-2011, 2011.

28) Hoffmann, T., Odum, J. R., Bowman, F., Collins, D., Klockow, D., Flagan, R. C., and Seinfeld, J. H.: Formation of organic aerosols from the oxidation of biogenic hydrocarbons, J. Atmos. Chem., 26, 189–222, 1997.

29) Intergovernmental Panel on Climate Change: Climate Change 2007: The Scientific Basis. Contribution of Working Group 1 to the Fourth Assessment Report of the Intergovernmental Panel on Climate Change, edited by: Solomon, S., Qin, D., Manning, M. Chen, Z., Marquis, M., Averyt, K. B., Tignor, M., and Miller, H. L., 996 pp., Cambridge Univ. Press, New York, 2007.

30) Jimenez, J. L., Canagaratna, M. R., Donahue, N. M., Prevot, A. S. H., Zhang, Q., Kroll, J. H., DeCarlo, P. F., Allan, J. D., Coe, H., Ng, N. L., Aiken, A. C., Docherty, K. S., Ulbrich, I. M., Grieshop, A. P., Robinson, A. L., Duplissy, J., Smith, J. D., Wilson, K. R., Lanz, V. A., Hueglin, C., Sun, Y. L., Tian, J., Laaksonen, A., Raatikainen, T., Rautiainen, J., Vaattovaara, P., Ehn, M., Kulmala, M., Tomlinson, J. M., Collins, D. R., Cubison, M. J., Dunlea, E. J., Huffman, J. A., Onasch, T. B., Alfarra, M. R., Williams, P. I., Bower, K., Kondo, Y., Schneider, J., Drewnick, F., Borrmann, S., Weimer, S., Demerjian, K., Salcedo, D., Cottrell, L., Griffin, R., Takami, A., Miyoshi, T., Hatakeyama, S., Shimono, A., Sun, J. Y., Zhang, Y. M., Dzepina, K., Kimmel, J. R., Sueper, D., Jayne, J. T., Herndon, S. C., Trimborn, A. M., Williams, L. R., Wood, E. C., Middlebrook, A. M., Kolb, C. E., Baltensperger, U. and Worsnop, D. R.: Evolution of organic aerosols in the atmosphere., Science, 326(5959), 1525–9, doi:10.1126/science.1180353, 2009.

31) Jung, J., Fountoukis, C., Adams, P. J. and Pandis, S. N.: Simulation of in situ ultrafine particle formation in the eastern United States using PMCAMx-UF, J. Geophys. Res., 115, D03203, doi:10.1029/2009JD012313, 2010.

32) Jungclaus, J. H., Lorenz, S. J., Timmreck, C., Reick, C. H., Brovkin, V., Six, K., and Marotzke, J.: Climate and carbon-cycle variability over the last millennium. Climate of the Past Discussions, 6, 1009-1044, 2010.

33) Kanakidou, M., Seinfeld, J. H., Pandis, S. N., Barnes, I., Dentener, F. J., Facchini, M. C., Van Dingenen, R., Ervens, B., Nenes, A., Nielsen, C. J., Swietlicki, E., Putaud, J. P., Balkanski, Y., Fuzzi, S., Horth, J., Moortgat, G. K., Winterhalter, R., Myhre, C. E. L., Tsigaridis, K., Vignati, E., Stephanou, E. G., and Wilson, J.: Organic aerosol and global climate modelling: a review, Atmos. Chem. Phys., 5, 1053–1123, doi:10.5194/acp-5-1053-2005, 2005.

34) Kanawade, V. P., Benson, D. R., and Lee, S.-H.: Statistical analysis of 4-year observations of aerosol sizes in a semi-rural continental environment, Atmos. Environ., 59, 30–38, 2012.

35) Kaplan, J. O., Krumhardt, K. M., Ellis, E. C., Ruddiman, W. F., Lemmen, C., & Goldewijk, K. K.: Holocene carbon emissions as a result of anthropogenic land cover change, The Holocene, 21(5), 775-791, 2011.

36) Kerminen, V.-M. and Kulmala, M.: Analytical formulae connecting the "real" and the "apparent" nucleation rate and the nuclei number concentration for atmospheric nucleation events, J. Aerosol Sci., 33, 609–622, 2002.

37) Kerminen, V.-M., Paramonov, M., Anttila, T., Riipinen, I., Fountoukis, C., Korhonen, H., Asmi, E., Laasko, L., Lihavainen, H., Sweitlicki, E., Svenningson, B., Asmi, A., Pandis, S. N., Kulmala, M., Petaja, T.: Cloud condensation nuclei production associated with atmospheric nucleation: a synthesis based on existing literature and new results, Atmospheric Chemistry and Physics, 12, 12037-12059, 2012.

38) Korhonen, P., Kulmala, M., Laaksonen, A., Viisanen, Y., McGraw, R., & Seinfeld, J. H.: Ternary nucleation of H2SO4, NH3, and H2O in the atmosphere. Journal of Geophysical Research: Atmospheres (1984–2012),104(D21), 26349-26353, 1999.

39) Kroll, J. H., Ng, N. L., Murphy, S. M., Flagan, R. C., and Seinfeld, J. H.: Secondary organic aerosol formation from isoprene photooxidation, Environ. Sci. Technol., 40, 1869–1877, doi:10.1021/Es0524301, 2006.

40) Kuang, C., McMurry, P. H. and McCormick, A. V: Determination of cloud condensation nuclei production from measured new particle formation events, Geophysical Research Letters, 36(9), n/a–n/a, doi:10.1029/2009GL037584, 2009.

41) Kuang, C., Chen, M., Zhao, J., Smith, J., McMurry, P. H. and Wang, J.: Size and time-resolved growth rate measurements of 1 to 5 nm freshly formed atmospheric nuclei, Atmospheric Chemistry and Physics, 12(7), 3573–3589, doi:10.5194/acp-12-3573-2012, 2012.

42) Kulmala, M., Vehkamäki, H., Petäjä, T., Dal Maso, M., Lauri, A., Kerminen, V. M., Birmili, W., and McMurry, P. H.: Formation and growth rates of ultrafine atmospheric particles: a review of observations, Journal of Aerosol Science,35(2), 143-176, 2004.

43) Kulmala, M., Pirjola, L. and Makela, J. M.: Stable sulphate clusters as a source of new atmospheric particles, Nature, 404(6773), 66-69, doi:10.1038/35003550, 2000.

44) Kulmala, M., Vehkam¨aki, H., Pet¨aj¨a, T., Dal Maso, M., Lauri, A., Kerminen, V.-M., Birmili, W., and McMurry, P. H.: Formation and growth of ultrafine atmospheric particles: A review of observations, J. Aerosol Sci., 35, 143–176, 2004.

45) Lane T. E. and S. N. Pandis (2007) Predicted secondary organic aerosol concentrations from the oxidation of isoprene in the Eastern United States, Environ. Sci. Tech., 41, 3984-3990.

46) Laothawornkitkul, J., Taylor, J. E., Paul, N. D., & Hewitt, C. N.: Biogenic volatile organic compounds in the Earth system, New Phytologist,183, 27-51, 2009.

47) Leaitch, W.R., S. Sharma, L. Huang, A. M. Macdonald, D. Toom-Sauntry, A. Chivulescu, K. von Salzen, J.R. Pierce, N.C. Shantz, A. Bertram, J. Schroder, A.-L. Norman, R.Y.-W. Change: Dimethyl Sulphide Control of the Clean Summertime Arctic Aerosol and Cloud: submitted to Elementa: Science of the Anthropocene, 2013.

48) Lee, Y. H. and Adams, P. J.: Evaluation of aerosol distributions in the GISS-TOMAS global aerosol microphysics model with remote sensing observations, Atmospheric Chemistry and Physics, 10(5), 2129–2144, doi:10.5194/acp-10-2129-2010, 2010.

49) Lee, L. A., Pringle, K. J., Reddington, C. L., Mann, G. W., Stier, P., Spracklen, D. V., Pierce, J. R., and Carslaw, K. S.: The magnitude and causes of uncertainty in global model simulations of cloud condensation nuclei, Atmos. Chem. Phys., 13, 8879-8914, doi:10.5194/acpd-13-8879-2013, 2013.

50) Levin, E. J. T., Kreidenweis, S. M., McMeeking, G. R., Carrico, C. M., Collett Jr., J. L. and Malm, W. C.: Aerosol physical, chemical and optical properties during the Rocky Mountain Airborne Nitrogen and Sulfur study, Atmospheric Environment, 43(11), 1932–1939, doi:10.1016/j.atmosenv.2008.12.042, 2009.

51) Levin, E. J. T., Prenni, a. J., Petters, M. D., Kreidenweis, S. M., Sullivan, R. C., Atwood, S. a., Ortega, J., DeMott, P. J. and Smith, J. N.: An annual cycle of size-resolved aerosol hygroscopicity at a forested site in Colorado, Journal of Geophysical Research, 117(D6), D06201, doi:10.1029/2011JD016854, 2012.

52) Lim, Y. B., Tan, Y., Perri, M. J., Seitzinger, S. P., and Turpin, B. J.: Aqueous chemistry and its role in secondary organic aerosol (SOA) formation, Atmos. Chem. Phys., 10, 10521–10539, doi:10.5194/acp-10-10521-2010, 2010.

53) Makkonen, R., Asmi, A., Kerminen, V. M., Boy, M., Arneth, A., Hari, P., & Kulmala, M.: Air pollution control and decreasing new particle formation lead to strong climate warming, Atmospheric Chemistry and Physics, 12, 1515-1524, 2010.

54) Manninen, H. E., Nieminen, T., Asmi, E., Gagné, S., Häkkinen, S., Lehtipalo, K., Aalto, P., Vana, M., Mirme, A., Mirme, S., Hõrrak, U., Plass-Dülmer, C., Stange, G., Kiss, G., Hoffer, A., Törő, N., Moerman, M., Henzing, B., de Leeuw, G., Brinkenberg, M., Kouvarakis, G. N., Bougiatioti, A., Mihalopoulos, N., O'Dowd, C., Ceburnis, D., Arneth, A., Svenningsson, B., Swietlicki, E., Tarozzi, L., Decesari, S., Facchini, M. C., Birmili, W., Sonntag, A., Wiedensohler, A., Boulon, J., Sellegri, K., Laj, P., Gysel, M., Bukowiecki, N., Weingartner, E., Wehrle, G., Laaksonen, A., Hamed, A., Joutsensaari, J., Petäjä, T., Kerminen, V.-M., and Kulmala, M.: EUCAARI ion spectrometer measurements at 12 European sites – analysis of new particle formation events, Atmos. Chem. Phys., 10, 7907-7927, doi:10.5194/acp-10-7907-2010, 2010.

55) MacFarling Meure, C., Etheridge, D., Trudinger, C., Steele, P., Langenfelds, R., Van Ommen, T., and Elkins, J.: Law Dome CO2, CH4 and N2O ice core records extended to 2000 years BP, Geophysical Research Letters, 33 , 2006.

56) McFiggans, G., Artaxo, P., Baltensperger, U., Coe, H., Facchini, M.C., Feingold, G., Fuzzi, S., Gysel, M., Laaksonen, A., Lohmann, U., Mentel, T.F., Murphy, D.M., O'Dowd, C.D., Snider, J.R., and Weingartner, E.: The effect of physical and chemical aerosol properties on warm cloud droplet activation. Atmos. Chem. Phys. 6, 2593–2649, 2006. http://www.atmos-chem-phys.net/6/2593/2006/.

57) Mäkelä, J. M., Aalto, P., Jokinen, V., Pohja, T., Nissinen, A., Palmroth, S., Markkanen, T., Seitsonen, K., Lihavainen, H. and Kulmala, M.: Observations of ultrafine aerosol particle formation and growth in boreal forest, Geophys. Res. Lett., 24(10), PP. 1219-1222, doi:199710.1029/97GL00920, 1997.

58) Merikanto, J., Spracklen, D. V., Mann, G. W., Pickering, S. J., and Carslaw, K. S.: Impact of nucleation on global CCN, Atmos. Chem. Phys., 9, 8601–8616, doi:10.5194/acp-9-8601-2009, 2009.

59) Metzger, A., Verheggen, B., Dommen, J., Duplissy, J., Prevot, A.S.H., Weingartner, E., Riipinen, I., Kulmala, M., Spracklen, D.V., Carslaw, K.S., and Baltensperger, U.,Atmospheric Chemistry Special Feature: Evidence for the role of organics in aerosol particle formation under atmospheric conditions, Proceedings of the National Academy of Sciences, doi:10.1073/pnas.0911330107, 2010.

60) Napari, I., Noppel, M., Vehkamäki, H. and Kulmala, M.: Parametrization of ternary nucleation rates for H2SO4-NH3-H2O vapors, Journal of Geophysical Research: Atmospheres, 107(D19), AAC 6–1–AAC 6–6, doi:10.1029/2002JD002132, 2002.

61) Ng, N. L., Canagaratna, M. R., Zhang, Q., Jimenez, J. L., Tian, J., Ulbrich, I. M., Kroll, J. H., Docherty, K. S., Chhabra, P. S., Bahreini, R., Murphy, S. M., Seinfeld, J. H., Hildebrandt, L., Donahue, N. M., DeCarlo, P. F., Lanz, V. A., Prevot, A. S. H., Dinar, E., Rudich, Y., and Worsnop, D. R.: Organic aerosol components observed in Northern Hemispheric datasets from Aerosol Mass Spectrometry, Atmos. Chem. Phys., 10, 4625–4641, doi:10.5194/acp-10-4625-2010, 2010.

62) Pankow, J. F.: An absorption model of gas/particle partitioning of organic compounds in the atmosphere, Atmos. Environ., 28, 185–188, 1994.

63) Peñuelas, J., & Staudt, M.: BVOCs and global change, Trends in plant science, 15(3), 133-144, 2010.

64) Petters, M. D. and Kreidenweis, S. M.: A single parameter representation of hygroscopic growth and cloud condensation nucleus activity, Atmos. Chem. Phys., 7, 1961-1971, doi:10.5194/acp-7-1961-2007, 2007.

65) Pierce, J. R. and Adams, P. J.: Global evaluation of CCN formation by direct emission of sea salt and growth of ultrafine sea salt, Journal of Geophysical Research-Atmospheres, 111(D6), D06203, doi:10.1029/2005JD006186, 2006.

66) Pierce, J. R. and Adams, P. J.: Efficiency of cloud condensation nuclei formation from ultrafine particles, Atmospheric Chemistry and Physics, 7, 1367–1379, 2007.

67) Pierce, J. R. and Adams, P. J.: A Computationally Efficient Aerosol Nucleation/ Condensation Method: Pseudo-Steady-State Sulfuric Acid, Aerosol Science and Technology, 43(3), 216–226, doi:10.1080/02786820802587896, 2009a.

68) Pierce, J. R. and Adams, P. J.: Can cosmic rays affect cloud condensation nuclei by altering new particle formation rates?, Geophysical Research Letters, 36(9), 1–6, doi:10.1029/2009GL037946, 2009b.

69) Pierce, J. R. and Adams, P. J.: Uncertainty in global CCN concentrations from uncertain aerosol nucleation and primary emission rates, Atmospheric Chemistry and Physics, 9(4), 1339–1356, doi:10.5194/acp-9-1339-2009, 2009c.

70) Pierce, J. R., Chen, K. and Adams, P. J.: Contribution of primary carbonaceous aerosol to cloud condensation nuclei: processes and uncertainties evaluated with a global aerosol microphysics model, Atmospheric Chemistry and Physics, 7, 5447–5466, 2007.

71) Pierce, J. R., Riipinen, I., Kulmala, M., Ehn, M., Petäjä, T., Junninen, H., Worsnop, D. R., and Donahue, N. M.: Quantification of the volatility of secondary organic compounds in ultrafine particles during nucleation events, Atmos. Chem. Phys., 11, 9019-9036, doi:10.5194/acp-11-9019-2011, 2011.

72) Pierce, J. R., Leaitch, W. R., Liggio, J., Westervelt, D. M., Wainwright, C. D., Abbatt, J. P. D., Ahlm, L., Al-Basheer, W., Cziczo, D. J., Hayden, K. L., Lee, A. K. Y., Li, S.-M., Russell, L. M., Sjostedt, S. J., Strawbridge, K. B., Travis, M., Vlasenko, A., Wentzell, J. J. B., Wiebe, H. A., Wong, J. P. S., and Macdonald, A. M.: Nucleation and condensational growth to CCN sizes during a sustained pristine biogenic SOA event in a forested mountain valley, Atmos. Chem. Phys., 12, 3147-3163, doi:10.5194/acp-12-3147-2012, 2012.

73) Pierce, J. R., Evans, M. J., Scott, C. E., D'Andrea, S. D., Farmer, D. K., Swietlicki, E., and Spracklen, D. V.: Weak global sensitivity of cloud condensation nuclei and the aerosol indirect effect to Criegee + SO2 chemistry, Atmos. Chem. Phys., 13, 3163-3176, doi:10.5194/acp-13-3163-2013, 2013.

74) Pongratz, J., Reick, C., Raddatz, T., & Claussen, M.: A reconstruction of global agricultural areas and land cover for the last millennium, Global Biogeochemical Cycles, 22, 2008.

75) Pongratz, J., Raddatz, T., Reick, C. H., Esch, M., and Claussen, M.: Radiative forcing from anthropogenic land cover change since AD 800, Geophysical Research Letters, 36(2), 2009.

76) Putaud, J. P., Raes, F., Van Dingenen, R., Bruggemann, E., Facchini, M. C., Decesari, S., Fuzzi, S., Gehrig, R., Huglin, C., Laj, P., Lorbeer, G., Maenhaut, W., Mihalopoulos, N., Mulller, K., Querol, X., Rodriguez, S., Schneider, J., Spindler, G., ten Brink, H., Torseth, K., and Wiedensohler, A.: European aerosol phenomenology-2: chemical characteristics of particulate matter at kerbside, urban, rural and background sites in Europe, Atmos. Environ., 38, 2579–2595, 2004.

77) Pye, H. O. T., Chan, A. W. H., Barkley, M. P., and Seinfeld, J. H.: Global modeling of organic aerosol: the importance of reactive nitrogen (NOx and NO3), Atmos. Chem. Phys., 10, 11261-11276, doi:10.5194/acp-10-11261-2010, 2010.

78) Reddington, C. L., Carslaw, K. S., Spracklen, D. V., Frontoso, M. G., Collins, L., Merikanto, J., Minikin, A., Hamburger, T., Coe, H., Kulmala, M., Aalto, P., Flentje, H., Plass-Dülmer, C., Birmili, W., Wiedensohler, A., Wehner, B., Tuch, T., Sonntag, A., O'Dowd, C. D., Jennings, S. G., Dupuy, R., Baltensperger, U., Weingartner, E., Hansson, H.-C., Tunved, P., Laj, P., Sellegri, K., Boulon, J., Putaud, J.-P., Gruening, C., Swietlicki, E., Roldin, P., Henzing, J. S., Moerman, M., Mihalopoulos, N., Kouvarakis, G., Ždímal, V., Zíková, N., Marinoni, A., Bonasoni, P., and Duchi, R.: Primary versus secondary contributions to particle number concentrations in the European boundary layer, Atmos. Chem. Phys., 11, 12007-12036, doi:10.5194/acp-11-12007-2011, 2011.

79) Rosenfeld, D., Lohmann, U., Raga, G. B., O'Dowd, C. D., Kulmala, M., Fuzzi, S., Reissell, A., and Andreae, M. O.: Flood or Drought: How Do Aerosols Affect Precipitation?, Science, 312, 1309–1313, 2008.

80) Riipinen, I., Pierce, J. R., Yli-Juuti, T., Nieminen, T., Häkkinen, S., Ehn, M., Junninen, H., Lehtipalo, K., Petäjä, T., Slowik, J., Chang, R., Shantz, N. C., Abbatt, J., Leaitch, W. R., Kerminen, V.-M., Worsnop, D. R., Pandis, S. N., Donahue, N. M., and Kulmala, M.: Organic condensation: a vital link connecting aerosol formation to cloud condensation nuclei (CCN) concentrations, Atmos. Chem. Phys., 11, 3865-3878, doi:10.5194/acp-11-3865-2011, 2011.

81) Scott, C. E., Rap, A., Spracklen, D. V., Forster, P. M., Carslaw, K. S., Mann, G. W., Pringle, K. J., Kivekäs, N., Kulmala, M., Lihavainen, H., and Tunved, P.: The direct and indirect radiative effects of biogenic secondary organic aerosol, submitted to Atmos. Chem. Phys. Disc., 2013.

82) Sipilä, M., Berndt, T., Petäjä, T., Brus, D., Vanhanen, J., Stratmann, F., Patokoski, J., Mauldin III, R. L., Hyvärinen, A.-P., Lihavainen, H., and Kulmala, M.: Role of Sulfuric Acid in Atmospheric Nucleation, Science, 327, 1243–1246, 2010.

83) Sitch, S., Smith, B., Prentice, I. C., Arneth, A., Bondeau, A., Cramer, W., Kaplan, J. O., Levis, S., Lucht, W., Sykes, M. T., Thonicke, K., and Venevsky, S.: Evaluation of ecosystem dynamics, plant geography and terrestrial carbon cycling in the LPJ dynamic global vegetation model. Global Change Biology, 9(2), 161-185, 2003.

84) Smith, B., Prentice, I. C., and Sykes, M. T.: Representation of vegetation dynamics in the modelling of terrestrial ecosystems: comparing two contrasting approaches within European climate space. Global Ecology and Biogeography,10(6), 621-637, 2001.

85) Snow-Kropla, E. J., Pierce, J. R., Westervelt, D. M. and Trivitayanurak, W.: Cosmic rays, aerosol formation and cloud-condensation nuclei: sensitivities to model uncertainties, Atmospheric Chemistry and Physics, 11(8), 4001–4013, doi:10.5194/acp-11-4001-2011, 2011.

86) Solomon, S., Qin, D., Manning, M., Chen, Z., Marquis, M., Averyt, K. B., Tignor, M., and Miller, H. L.: Climate Change 2007: The Physical Science Basis. Contribution of Working Group I to the Fourth Assessment Report of the Intergovernmental Panel on Climate Change, Cambridge University Press, New York, NY, USA, 2007.

87) Spracklen, D. V., Carslaw, K. S., Kulmala, M., Kerminen, V.-M., Mann, G. W., and Sihto, S.-L.: The contribution of boundary layer nucleation events to total particle concentrations on regional and global scales, Atmos. Chem. Phys., 6, 5631-5648, doi:10.5194/acp-6-5631-2006, 2006.

88) Spracklen, D. V, Carslaw, K. S., Kulmala, M., Kerminen, V. M., Sihto, S. L., Riipinen, I., Merikanto, J., Mann, G. W., Chipperfield, M. P., Wiedensohler, A., Birmili, W., and Lihavainen, H.: Contribution of particle formation to global cloud condensation nuclei concentrations, Geophys. Res. Lett., 35, D06808, doi:10.1029/2007GL033038, 2008.

89) Spracklen, D. V., Carslaw, K. S., Poschl, U., Rap, A., and Forster, P. M.: Global cloud condensation nuclei influenced by carbonaceous combustion aerosol, Atmos. Chem. Phys., 11, 9067–9087, doi:10.5194/acp-11-9067-2011, 2011a.

90) Spracklen, D. V., Jimenez, J. L., Carslaw, K. S., Worsnop, D. R., Evans, M. J., Mann, G. W., Zhang, Q., Canagaratna, M. R., Allan, J., Coe, H., McFiggans, G., Rap, A., and Forster, P.: Aerosol mass spectrometer constraint on the global secondary organic aerosol budget, Atmos. Chem. Phys., 11, 12109-12136, doi:10.5194/acp-11-12109-2011, 2011b.

91) Stanier, C. O., Khlystov, A. Y., and Pandis, S. N.: Ambient aerosol size distributions and number concentrations measured during the Pittsburgh Air Quality Study (PAQS), Atmos. Environ., 38, 3275–3284, 2004.

92) Trivitayanurak, W., Adams, P. J., Spracklen, D. V and Carslaw, K. S.: Tropospheric aerosol microphysics simulation with assimilated meteorology: model description and intermodel comparison, Atmospheric Chemistry and Physics, 8(12), 3149–3168, 2008.

93) Twomey, S.: Aerosols, Clouds, and Radiation, Atmos. Environ., 25A, 2435-2442, 1991.

94) Twomey, S.: The Influence of Pollution on the Shortwave Albedo of Clouds, J. Atmos. Sci., 34, 1149–1152, 1977.

95) Twomey, S.: Pollution and the Planetary Albedo, Atmos. Environ., 8, 1251-1256, 1974.

96) Van Donkelaar, A., Martin, R. V., Leaitch, W. R., Macdonald, A. M., Walker, T. W., Streets, D. G., Zhang, Q., Dunlea, E. J., Jimenez, J. L., Dibb, J. E., Huey, L. G., Weber, R., and Andreae, M. O.: Analysis of aircraft and satellite measurements from the Intercontinental Chemical Transport Experiment (INTEX-B) to quantify long-range transport of East Asian sulfur to Canada, Atmos. Chem. Phys., 8, 2999–3014, doi:10.5194/acp-8-2999-2008, 2008.

97) Vehkamaki, H., Napari, I., Kulmala, M. and Noppel, M.: Stable ammonium bisulfate clusters in the atmosphere, Physical Review Letters, 93(14), doi:10.1103/PhysRevLett.93.148501 [online] Available from: ://000224211900081, 2004.

98) Vehkamäki, H. and Riipinen, I.: Thermodynamics and kinetics of atmospheric aerosol particle formation and growth, Chemical Society Reviews, 41(15), 5160-5173, doi: 10.1039/c2cs00002d, 2012.

99) Volkamer, R., Jimenez, J. L., San Martini, F., Dzepina, K., Zhang, Q., Salcedo, D., Molina, L. T., Worsnop, D. R., Molina, M. J.: Secondary organic aerosol formation from anthropogenic air pollution: Rapid and higher than expected, Geophysical Research Letters, 33(17), 2006.

100) Wainwright, C. D., Pierce, J. R., Liggio, J., Strawbridge, K. B., Macdonald, A. M., and Leaitch, R. W.: The effect of model spatial resolution on Secondary Organic Aerosol predictions: a case study at Whistler, BC, Canada, Atmos. Chem. Phys., 12, 10911-10923, doi:10.5194/acp-12-10911-2012, 2012.

101) Wang, S. C. and Flagan, R. C.: Scanning Electrical Mobility Spectrometer. Aerosol Science and Technology, 1990. 13(2): p. 230-240.

102) Wang, M. and Penner, J. E.: Aerosol indirect forcing in a global model with particle nucleation, Atmos. Chem. Phys., 9, 239-260, doi:10.5194/acp-9-239-2009, 2009.

103) Wang, L., Khalizov, A. F., Zheng, J.. Xu, W., Ma, Y., Lal, V., and Zhang, R.: Atmospheric nanoparticles formed from heterogeneous reactions of organics, Nature Geosci., 3, 238–242, 2010.

104) Westervelt, D. M., Pierce, J. R., Riipinen, I., Trivitayanurak, W., Hamed, A., Kulmala, M., Laaksonen, A., Decesari, S., and Adams, P. J.: Formation and growth of nucleated particles into cloud condensation nuclei: model-measurement comparison, Atmos. Chem. Phys. Discuss., 13, 8333-8386, doi:10.5194/acpd-13-8333-2013, 2013.

105) Yli-Juuti, T., Nieminen, T., Hirsikko, A., Aalto, P. P., Asmi, E., Hõrrak, U., Manninen, H. E., Patokoski, J., Dal Maso, M., Petäjä, T., Rinne, J., Kulmala, M., and Riipinen, I.: Growth rates of nucleation mode particles in Hyytiälä during 2003−2009: variation with particle size, season, data analysis method and ambient conditions, Atmos. Chem. Phys., 11, 12865-12886, doi:10.5194/acp-11-12865-2011, 2011.

106) Zhang, Q., Jimenez, J. L., Canagaratna, M. R., Allan, J. D., Coe, H., Ulbrich, I., Alfarra, M. R., Takami, A., Middlebrook, A. M., Sun, Y. L., Dzepina, K., Dunlea, E., Docherty, K., De-Carlo, P. F., Salcedo, D., Onasch, T., Jayne, J. T., Miyoshi, T., Shimono, A., Hatakeyama, S., Takegawa, N., Kondo, Y., Schneider, J., Drewnick, F., Borrmann, S., Weimer, S., Demerjian, K., Williams, P., Bower, K., Bahreini, R., Cottrell, L., Griffin, R. J., Rautianinen, J., Sun, J. Y., Zhang, Y. M., and Worsnop, D. R.: Ubiquity and dominance of oxygenated species in organic aerosols in anthropogenically-influenced Nothern Hemisphere midlatitudes, Geophys. Res. Lett., 34, L13801, doi:10.1029/2007GL029979, 2007.

107) Zhang, Q., Jimenez, J. L., Canagaratna, M. R., Ulbrich, I. M., Ng, N. L., Worsnop, D. R., and Sun, Y. L.: Understanding atmospheric organic aerosols via factor analysis of aerosol mass spectrometry: a review, Anal. Bioanal. Chem., 401, 3045–3067, doi:10.1007/s00216-011-5355-y, 2011.

108) Zhang, X., Pandis, S. N. and Seinfeld, J. H.: Diffusion-Limited Versus Quasi-Equilibrium Aerosol Growth, Aerosol Science and Technology, 46(8), 874–885, doi:10.1080/02786826.2012.679344, 2012.

APPENDIX A COPYRIGHT PERMISSION LETTER

The following regulations are reproduced from Atmospheric Chemistry and Physics (http://www.atmospheric-chemistry-and-physics.net/general_information/license_and_copyright.html):

The following License and Copyright Agreement is valid for any article published by Copernicus Publications on behalf of the European Geosciences Union (EGU) in the journal Atmospheric Chemistry and Physics and its discussion forum Atmospheric Chemistry and Physics Discussions whose original manuscript was received from **10 December 2007** on.

Author's Certification

In submitting the manuscript, the authors certify that:

- They are authorized by their co-authors to enter into these arrangements.
- The work described has not been published before (except in the form of an abstract or proceedings-type publication – including discussion papers – or as part of a published lecture or thesis), that it is not under consideration for publication elsewhere, that its publication has been approved by all the author(s) and by the responsible authorities – tacitly or explicitly – of the institutes where the work has been carried out.
- They secure the right to reproduce any material that has already been published or copyrighted elsewhere.
- They agree to the following license and copyright agreement:

Copyright

- Copyright on any article is retained by the author(s). Regarding copyright transfers please see below.
- Authors grant Copernicus Publications a license to publish the article and identify itself as the original publisher.
- Authors grant Copernicus Publications commercial rights to produce hardcopy volumes of the journal for sale to libraries and individuals.
- Authors grant any third party the right to use the article freely as long as its original authors and citation details are identified.
- The article and any associated published material is distributed under the Creative Commons Attribution 3.0